

(NASA-CR-146857) COORDINATED ANALYSIS OF
VARIOUS AURORAL MEASUREMENTS MADE DURING
NASA'S 1968 AND 1969 AIRBORNE AURORAL
EXPEDITIONS Final Report, 1 Jan. 1973 - 31
Dec. 1975 (Alaska Univ., College.) 101 p HC G3/46

N76-21802
HC \$5.50
Unclas
25211

GEOPHYSICAL INSTITUTE

of the

UNIVERSITY OF ALASKA

COORDINATED ANALYSIS OF VARIOUS AURORAL MEASUREMENTS
MADE DURING NASA'S 1968 AND 1969 AIRBORNE AURORAL EXPEDITIONS

FINAL REPORT

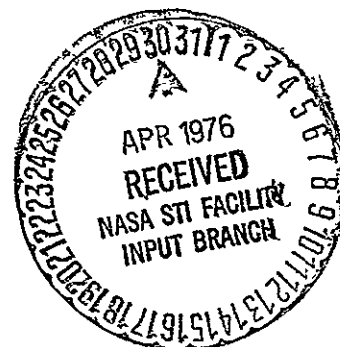
Grant NGR 02-001-099

Contract Period: January 1, 1973 to December 31, 1975

April 1976

Prepared for

NATIONAL AERONAUTICS AND SPACE ADMINISTRATION
AMES RESEARCH CENTER



3
1
3

GEOPHYSICAL INSTITUTE
of the
UNIVERSITY OF ALASKA

COORDINATED ANALYSIS OF VARIOUS AURORAL MEASUREMENTS
MADE DURING NASA'S 1968 AND 1969 AIRBORNE AURORAL EXPEDITIONS

FINAL REPORT

Grant NGR 02-001-099

Contract Period: January 1, 1973 to December 31, 1975

April 1976

Prepared for
NATIONAL AERONAUTICS AND SPACE ADMINISTRATION
AMES RESEARCH CENTER



GEOPHYSICAL INSTITUTE
of the
UNIVERSITY OF ALASKA

COORDINATED ANALYSIS OF VARIOUS AURORAL MEASUREMENTS
MADE DURING NASA'S 1968 AND 1969 AIRBORNE AURORAL EXPEDITIONS

FINAL REPORT

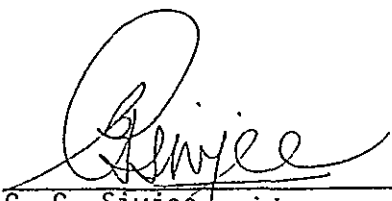
Grant NGR 02-001-099.

Contract Period: January 1, 1973 to December 31, 1975

April 1976

Prepared for

NATIONAL AERONAUTICS AND SPACE ADMINISTRATION
AMES RESEARCH CENTER



G. G. Sivjee
Principal Investigator

ABSTRACT

This report presents results from a coordinated analysis of some of the auroral optical measurements made by five different research groups aboard NASA's CV 990. The measurements analyzed form a small part of extensive spectroscopic, photometric and photographic data gathered during the 1968 and 1969 Airborne Auroral Expeditions. Simultaneous particle measurements from ESRO 1A satellite were used in the analysis. Because of the lack of close coordination among different experimenters, and wide differences in their data format and recording methods, only part of the large amount of data gathered during the two expeditions could be combined to study a few of the outstanding problems in magnetospheric and aeronomic physics. However, the coordinated analysis of even such a very limited data set has yielded scientifically interesting and important information about magnetospheric boundaries, interaction between magnetosheath particles and the terrestrial ionosphere, the polar bulge in helium abundance and excitation mechanisms of the triplet state of atmospheric N_2 in auroras. These results have been reported in scientific journals in the form of three separate articles. Further analysis of the data is required to elucidate the relation between 3466 and 5200 Å emissions of NI and the excitation of 3726-3729 Å emissions from atomic oxygen ions in auroras.

It is recommended that, in the future, experimenters attempt to coordinate their measurements so as to cover the largest possible spectrum of the auroral electromagnetic radiation simultaneously. They should also organize their data sets in one standard format and record them in a manner which will facilitate a coordinated analysis of all measurements.

INTRODUCTION

Detailed description of various measurements from the 1968 and 1969 Airborne Auroral Expeditions (AAE), made available for this project, has been given in a previous report (Sivjee, 1973). Organization, retrieval and filtering of all the data to identify sections suitable for coordinated analysis are also described in that report. Hence, this final report presents only the results of the analysis performed so far and sketches the scientific basis for continuing the work. A critical evaluation of the past airborne auroral expeditions appears at the end of the report together with some suggestions on how to organize the experiments on future missions for optimum scientific output.

ANALYSIS

The flights, originating from Bodo, to the mid-day auroral region produced the most interesting results. Color all-sky camera pictures of the mid-day aurora taken by the Alaska group, the photometric measurements of researchers from Johns Hopkins University, Boston College and Lockheed Company, spectroscopic measurements of the Colorado group and simultaneous particle data from ESRO 1A satellite were combined to study various magnetospheric boundaries and the interactions between magnetosheath particles and the ionosphere. Results of the analyses have been reported in two papers (Sivjee and Hultqvist, 1975; Sivjee, 1976). Measurements made by the same groups in a Westward Traveling Surge were analyzed to study the excitation of atmospheric N_2 by combining the measurements with computer model calculations (Rees et al., 1976). A summary of scientific information gathered from all these analyses are presented in the following section.

TABLE OF CONTENTS

	Page
ABSTRACT	i
INTRODUCTION	ii
ANALYSIS	iii
TABLE OF CONTENTS	iv
FIGURE CAPTIONS	v
LIST OF TABLES	vii
I. PARTICLE AND OPTICAL MEASUREMENTS IN THE MAGNETIC NOON SECTOR OF THE AURORAL OVAL	1
A. INTRODUCTION	1
B. PARTICLE MEASUREMENTS	1
C. OPTICAL MEASUREMENTS	6
D. COMPARISON OF RESULTS FROM ESRO IA PARTICLE MEASUREMENTS WITH CV 990 PHOTOMETRIC OBSERVATIONS	10
E. CONCLUSION	14
II. OPTICAL EMISSIONS FROM THE MID-DAY AURORA	15
A. INTRODUCTION	15
B. EXPERIMENTAL	15
C. ANALYSIS	22
1. Interaction of Magnetosheath Protons with the Atmosphere	23
2. Electron Interaction with the Atmosphere	26
3. Resonant Scattering of Sunlight by N_2^+ Ions	28
4. Auroral Emissions Around 3886 Å	29
D. SUMMARY	35
III. STUDIES OF MOLECULAR NITROGEN BANDS FROM AIRBORNE AURORAL SPECTROSCOPY	37
A. INTRODUCTION	37
B. INSTRUMENTATION AND CALIBRATION	38
C. OBSERVATIONS	40
D. ANALYSIS	55
1. The N_2 2PG System	60
2. The N_2 1PG System	60
3. The N_2 V-K System	66
4. [NI] 3466	72
5. Other Atomic Features	73
F. DISCUSSION AND CONCLUSIONS	73
IV. [OII] 3726-3729Å EMISSIONS FROM AURORAS	76
V. EXCITATION OF NI 3466 AND 5200 EMISSIONS	83
VI. OPTICAL EMISSION FROM O_2 , NO AND OTHER SPECIES IN A WESTWARD TRAVELING SURGE	84
VII. SUMMARY	85
ACKNOWLEDGMENTS	87
REFERENCES	88

FIGURE CAPTIONS

	Page
Figure 1. Particle data from orbit 6273 of ESRO IA satellite.	3
Figure 2. Photometric observations of the mid-day aurora from NASA's CV 990 jet aircraft.	7
Figure 3. Photometrically derived characteristic energy of electrons precipitating around the noon sector of the oval.	9
Figure 4. Tracts of the Convair 990 aircraft and the ESRO IA satellite during the mid-day auroral observations. Projections of various magnetospheric boundaries on the ionosphere deduced from particle and photometric measurements are also shown on the invariant latitude grid.	11
Figure 5. H_{β} intensity calculated from ESRO IA proton data and that observed from airborne photometric detectors.	12
Figure 6. Tracks of the Convair 990 and the ESRO IA satellite during the mid-day auroral observations on December 13, 1969, are shown on an invariant latitude grid.	17
Figure 7. Time history (or spatial variation) of some of the photometrically observed auroral emission features. The geometric shadow height is also shown.	18
Figure 8. Sum of 18, 100-sec spectrophotometer scans obtained during the mid-day auroral observations.	20
Figure 9. Thirty minute average of spectra between 3850A and 3920A obtained during mid-day auroral observations.	21
Figure 10. Synthetic spectra of N_2^+ ING bands for various population ratios of the $v^2 = 0$ and $v = 1$ levels of $N_2(X^1\Sigma_g^+)$ and $N_2(B^2\Sigma_u^+)$. The observed spectral profile is drawn assuming that the feature around 3886A is N_2^+ ING (1,1) band.	30
Figure 11. All-sky camera photograph of the aurora studied in this report. The circle indicates the field of view of the spectrometers, and the multichannel photometer.	41
Figure 12. Time history of the emission rates of three auroral spectral features obtained with a multichannel photometer. The two minute interval chosen for spectral analysis is indicated by the vertical lines.	42

FIGURE CAPTIONS (Cont'd)

	Page
Figure 13. Analog display of a twenty-five second spectral scan in the near UV obtained with the half-meter Ebert spectrophotometer at 5A resolution.	43
Figure 14. Analog display of an eight second spectral scan in the near IR obtained with the one-meter Ebert spectrophotometer at 15A resolution.	44
Figure 15. Two-minute average of five near UV spectra used in the analysis described in this report. Noise was removed by appropriate high frequency filtering. The location of all spectral features in the wavelength region 3100 to 4000 A is shown, whether or not they are actually present in the observed spectrum.	51
Figure 16. Two minute average of 18 near IR spectra used in the analysis described in this report. Noise was removed by appropriate high frequency filtering.	52
Figure 17. Spectral profile of the N_2^+ 1NG (0,0) and (1,1) bands obtained during the two minute auroral event used in the analysis. Synthetic band profiles corresponding to different vibrational and rotational temperatures have been superposed. A triangular shape with a half width of 5A for each rotational line has been assumed.	53
Figure 18. Differential spectra of secondary electrons derived from the model that describes the auroral event investigated in this report. Spectra at several altitudes are shown.	58
Figure 19. Excitation cross section for the N_2 $C^2\Pi_u$ state. Chung and Lin's (1973) and Cartwright's ^u (1973, 1975) results are derived theoretically while the results of the other three references are derived from laboratory experiments.	61
Figure 20. Excitation cross sections for the N_2 $B^3\Pi_g$ state. The results of Chung and Lin (1973) and ² of Cartwright (1973) are derived theoretically while the results of Shemansky and Broadfoot (1971a) and Stanton and St. John (1969) are derived from laboratory experiments.	62
Figure 21. Cross sections for the excitation of various v' levels of N_2 $B^3\Pi_g$ using peak values obtained by Shemansky and Broadfoot ^g (1971a) from laboratory measurements.	63

ORIGINAL PAGE IS
OF POOR QUALITY

FIGURE CAPTIONS (Cont'd)

	Page
Figure 22. Comparison between observed and predicted emission rates of several bands of the N_2 1PG system. Circles with error bars refer to the observations, while the crosses are the emission rates derived using the apparent excitation cross sections of Shemansky and Broadfoot (1971a). The pluses refer to the cascade component from the C state.	67
Figure 23. Excitation cross sections for the N_2 $A^3\Sigma_u^+$ state according to one laboratory measurement (Borst, 1972) and two theoretical computations.	71

LIST OF TABLES

	Page
<u>Section II</u>	
Table I. Observed Photon Emission Rates	19
Table II. Predicted Intensities of Optical Emissions Excited by Magnetosheath Electrons in the Cusp Region	28
<u>Section III</u>	
Table 1. N_2^+ 1NG	46
Table 2. N_2 2PG	47
Table 3. N_2 1PG	48
Table 4. N_2 V-K	49
Table 5. Atomic Features	56
Table 6. Neutral Model Atmosphere	64
Table 7. N_2 1PG	65
Table 8. Population Rates	68

I. PARTICLE AND OPTICAL MEASUREMENTS IN THE MAGNETIC NOON SECTOR OF THE AURORAL OVAL

A. INTRODUCTION

The intensity ratios of OI 6300Å to OI 5577Å and N_2^+ 4278Å auroral emissions provide some indication of the characteristic energy of auroral electrons (Rees and Luckey, 1974). This suggests a simple photometric method for mapping various parts of the auroral region (Eather and Mende, 1971). In particular, the photometric technique may be applied to observe the Magnetospheric Dayside Cleft (Eather and Mende, 1972; Peterson and Shepherd, 1974). However, in order to establish the optical measurements as a viable method for mapping various magnetospheric boundaries, it must be demonstrated that the results derived from such measurements tally with direct particle measurements.

Heikkilä et al. (1972) compared airborne photometric measurements with satellite particle observations from the noon sector made earlier in time; the two sets of data were not acquired simultaneously from the same location. In this paper we present auroral particle measurements from ESRO 1A satellite which were taken simultaneously with airborne photometric observations of the mid-day aurora. These are analyzed to delineate and compare various magnetospheric boundaries implied by the variations in the particle flux and the photometric intensities.

B. PARTICLE MEASUREMENTS

The ESRO 1A satellite carried various fixed energy electron and proton detectors, each having a square field of view of 8° half angle and a bandpass equal to 10% of the center energy. Their conversion factors were within the range 3.7×10^3 to 5×10^5 particles/(cm²-sec-sr-keV)

per count/sec (Riedler et al., 1970). The electron detectors responded to 1.3, 2.9, 5.8 and 13.3 keV electrons at 10° pitch angle (PA), and 1.4, 6.3 and 13.1 keV electrons at 80° PA. The proton detectors monitored 5.8 keV protons at 10° PA and 1.4 and 6.3 keV protons at 80° PA. The relative flux of particles of a given energy at 10° and 80° pitch angles can be interpreted to separate regions of magnetospheric trapped (mirroring) and precipitating particles.

Figure 1 shows ESRO IA particle measurements during part of orbit 6273. These measurements were made on December 13, 1969 between UT 0822 and 0828 during magnetically quiet conditions ($K_p=1^-$). Each data point in Figure 1 represents the average of all readings from a specific channel during a period of 8 seconds which approximately corresponds to a spatial extent of about 0.5° in Invariant Latitude (IL). Data points flagged with arrows represent the upper limit of the particle flux while the right- and left-most data points mark the boundaries outside which the particle flux was less than the sensitivity threshold of the detectors.

For the period covered by the measurements shown in Figure 1 the satellite height varied from 600 to 500 kms, while the angle between the sun and the field of view of all particle detectors was greater than 80° ; the latter rules out the possibility of any solar UV contamination of the particle data.

The particle information of prime interest in this paper related to magnetospheric cusp boundaries. In Figure 1 we note that the flux of precipitating electrons (i.e., when flux at 10° PA \gtrsim flux 80° PA) with energy greater than 1 keV decreased by more than an order of magnitude between IL 77 and 78° . Simultaneously the flux of precipitating protons

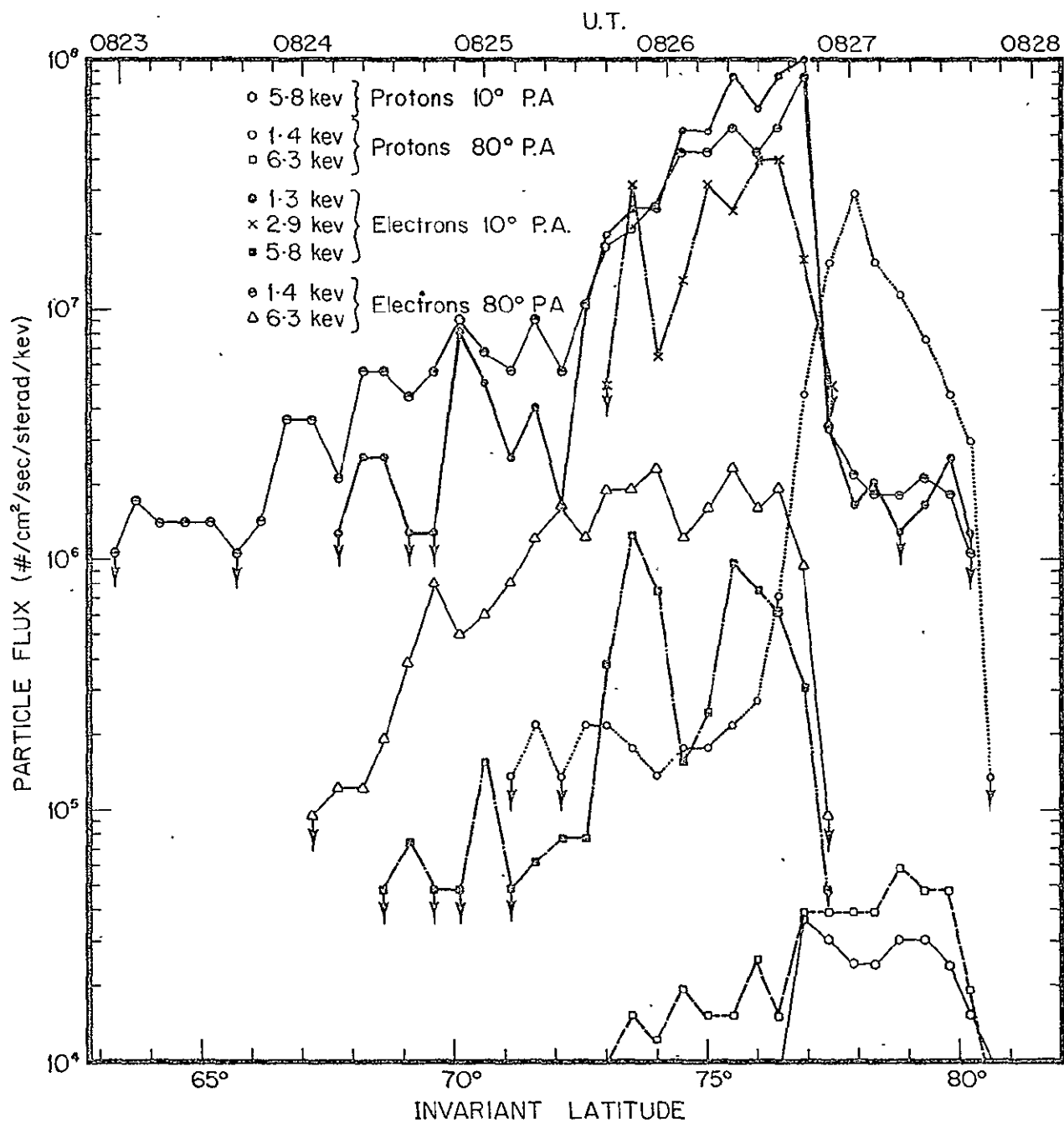


Figure 1

(as judged by the near equality of the 5.8 kev proton flux at 10° and 80° PA) increased drastically with the flux at 1.4 kev rising by almost two orders of magnitude. Assuming that the pitch angle distribution, over the lower hemisphere, of the precipitating proton flux is the same at all proton energies, the isotropic distribution of 5.3 kev protons suggests that the flux of 1.4 kev protons at 10° PA was the same as at 80° PA. Hence, in this region the flux of precipitating protons must peak at or below 1.4 kev. The boundary around IL 77 to 78° , where sharp changes in the flux of precipitating electrons and protons are evident, is interpreted as the last closed geomagnetic field line (Winningham, 1971) with magnetosheath particles precipitating poleward of it (Gladyshev et al., 1974). The spatial extent of the relatively soft flux (peaked at ≤ 1.4 kev) of magnetosheath protons is identified as the cusp region. Hence, on December 13, 1969 the cusp region around local magnetic noon was confined within $77.5^\circ \leq \text{IL} \leq 80.5^\circ$. According to the ESRO IA particle data the energy distribution of electrons precipitating in the cusp must have peaked well below 1 kev since the electron flux at 1.3 kev was barely above the detector threshold while the flux at higher energies was well below the sensitivity range of the detectors.

In addition to identifying the cusp region, the ESRO IA particle data contain information on other magnetospheric regions. In Figure 1 we note that equatorward of IL 70° only the 80° PA electron channel registered particle flux while the 10° PA channels did not detect any precipitation. The presence of only mirroring particles (in Van Allen belt) south of IL 70° can be interpreted to delineate the poleward boundary of the trapped zone. On the basis of previous analysis of ESRO

REPRODUCIBILITY OF THE
ORIGINAL PAGE IS POOR

I/AURORAE satellite particle measurements from the nighttime sector of the oval by Deehr et al. (1971), the present limited data indicates that around local magnetic noon on December 13, 1969 this boundary was at IL 70°. Between IL 70 and 77° there appears to have been precipitation of electrons with characteristic energy in the kev range, much higher than the value attributed to magnetosheath electrons precipitating along the cleft (Winningham, 1971). Most probably, they were the remnants of electrons, injected on the night side of the oval from the neutral plasma sheet, which had drifted to the mid-day section of the oval (Hultqvist, 1974).

In Figure 1, the loss cone in the region $70^\circ \leq IL \leq 77^\circ$ appears to be more depleted for 6.3 kev compared to 1.3 kev electrons, and the energy distribution of electrons changes with increasing IL (Hultqvist, 1974). The flux of these precipitating electrons decreases as we move south.

In summary, for the magnetic local noon region on December 13, 1969, the ESRO IA particle data furnish the following information about various magnetospheric regions:

- (1) Cusp: $77.5^\circ \leq IL \leq 80.5^\circ$. Region of precipitation of magnetosheath particles.
- (2) $70^\circ \leq IL \leq 77.5^\circ$: Precipitation of particles which have drifted from the nightside to the noon sector.
- (3) Poleward boundary of the stable trapped region: IL 70°.

The above demarcations of the cusp and other magnetospheric regions agree with corresponding values, for magnetically quiet conditions, derived by Winningham (1971) from ISIS particle data and by Deehr et al. (1971) from ESRO I/AURORAE satellite data.

C. OPTICAL MEASUREMENTS

Photometric measurements of OI 5577A and 6300A, H_β and N_2^+ 4278A emissions in the mid-day aurora were made both with a multichannel and tilting photometers (Dick et al., 1971; Eather and Mende, 1971). These observations were carried out from aboard NASA's CV 990 jet aircraft during NASA's 1969 Auroral Airborne Expedition on a flight that originated in Bodo, Norway, on December 13, 1969 UT (Sivjee and Rees, 1975). Zenith intensities of auroral emissions monitored between UT 0800 and 0900 are displayed in Figure 2. We note that south of IL 76.5° the intensity (I) of 5577A was greater than 6300A emission and the average ratios of $I(6300)/I(5577)$ and $I(6300)/I(4278)$ were 0.4 and 2.7. Between IL 76.5° and 78° the intensity of 5577 decreased relative to 6300 intensity and $I(6300)/I(5577)$ and $I(6300)/I(4278)$ ratios increased to 1.3 and 9.0, respectively. Poleward of IL 78° there was a dramatic strengthening of 6300A intensity relative to the intensities of both 5577 and 4278A. This accounts for the red patches recorded by the color all-sky camera aboard the CV 990 (Heikkila et al., 1972; Sivjee and Rees, 1975). The $I(6300)/I(5577)$ and $I(6300)/I(4278)$ ratios in the region $78^\circ \leq IL \leq 81^\circ$ were 4.4 and 25.9. In this last region there was also a steady H_β emission which attained a broad-peak value of 10R (Eather and Mende, 1971).

In Figure 2 the spatial extent as well as spatial and/or temporal variations in the intensities of OI 6300A and N_2^+ 4278A emissions contrast markedly with the limited extent, and steady nature, of hydrogen Balmer β emission at 4861A. Hence, the bulk of 5577, 6300 and 4278 emissions must originate from excitation of atmospheric constituents by

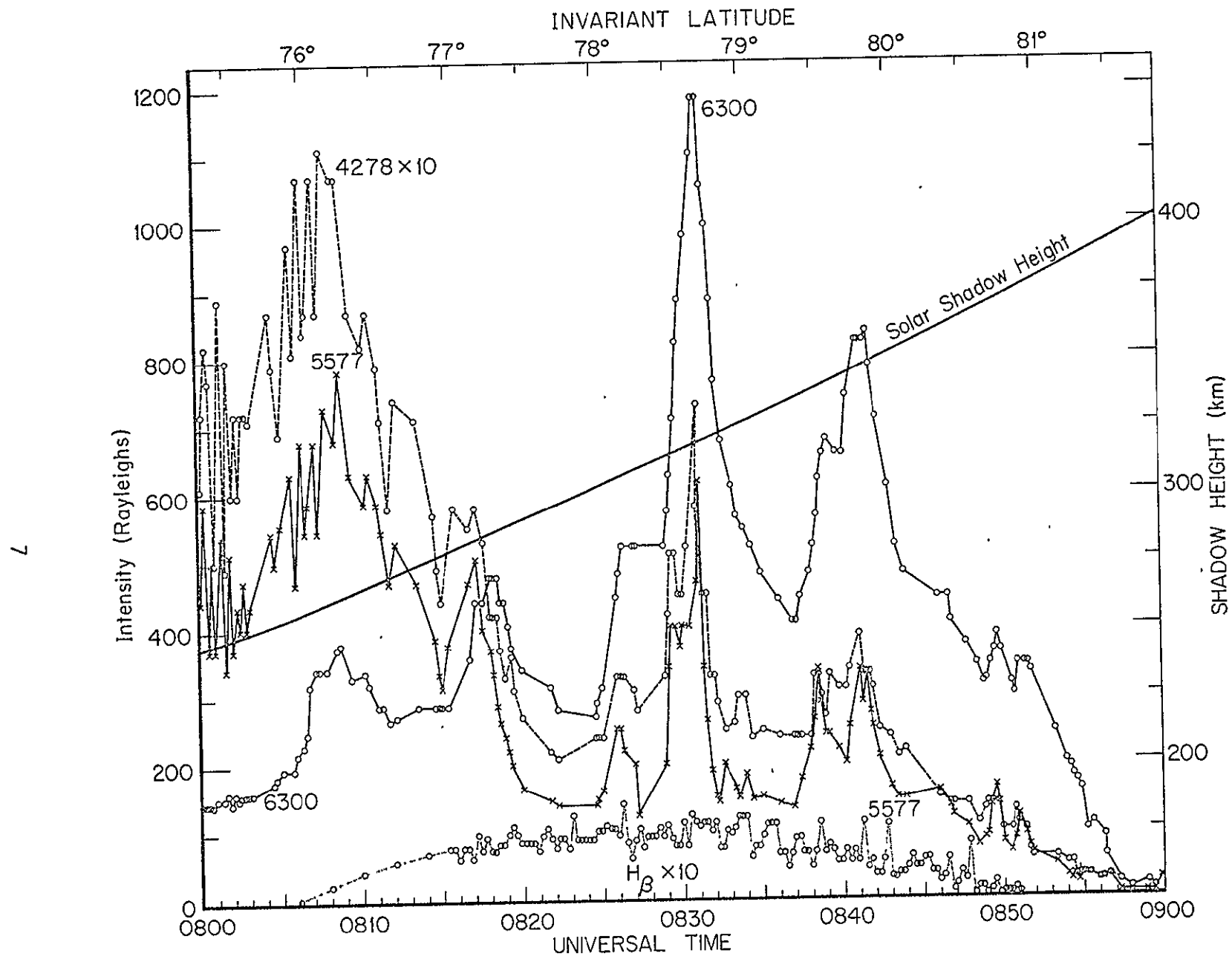


Figure 2

precipitating electrons and the secondary electrons resulting from such interactions. The contribution of proton generated secondary electrons to the excitation of OI 5577 and 6300 is negligible. The 4278 intensity resulting from magnetosheath proton precipitation is also small. We can assess $I(6300)$, $I(5577)$ and $I(4278)$ during proton precipitation from photometric measurements of H_β intensity (Eather, 1968; Sivjee, 1976). The net electron component of the two emissions can then be analyzed, in conjunction with Rees and Luckey's (1974) calculations, to estimate the characteristic energy of the precipitating electrons. (The energy distribution of the electron flux (F) is assumed to be Maxwellian, i.e., $F(E) = AE e^{-E/\alpha}$, where E is electron energy and α - the energy of peak electron flux - is loosely referred to as the characteristic energy.)

Figure 3 displays the characteristic energy, α , of electrons, precipitating around the magnetic noon sector of the auroral oval, derived from the above analysis of photometric data. Around local magnetic noon on December 13, 1969 the electrons precipitating in the region south of IL 76.5° had a characteristic energy of about 1.1 keV. This value decreased to 700 eV between IL 76.5 and about 78° . In the region of steady proton precipitation (as surmized from H_β emission) $78^\circ \leq IL \leq 81^\circ$, the electron flux was highly variable but its characteristic energy remained steady at around 250 eV. This area of both proton and soft electron (~ 250 eV) precipitations would correspond to the cusp region during magnetically quiet conditions (Winningham, 1971; Gladyshev et al., 1974).

In summary, the photometric data from the noon sector of the auroral oval, during magnetically quiet conditions, point to three different regions of particle precipitation:

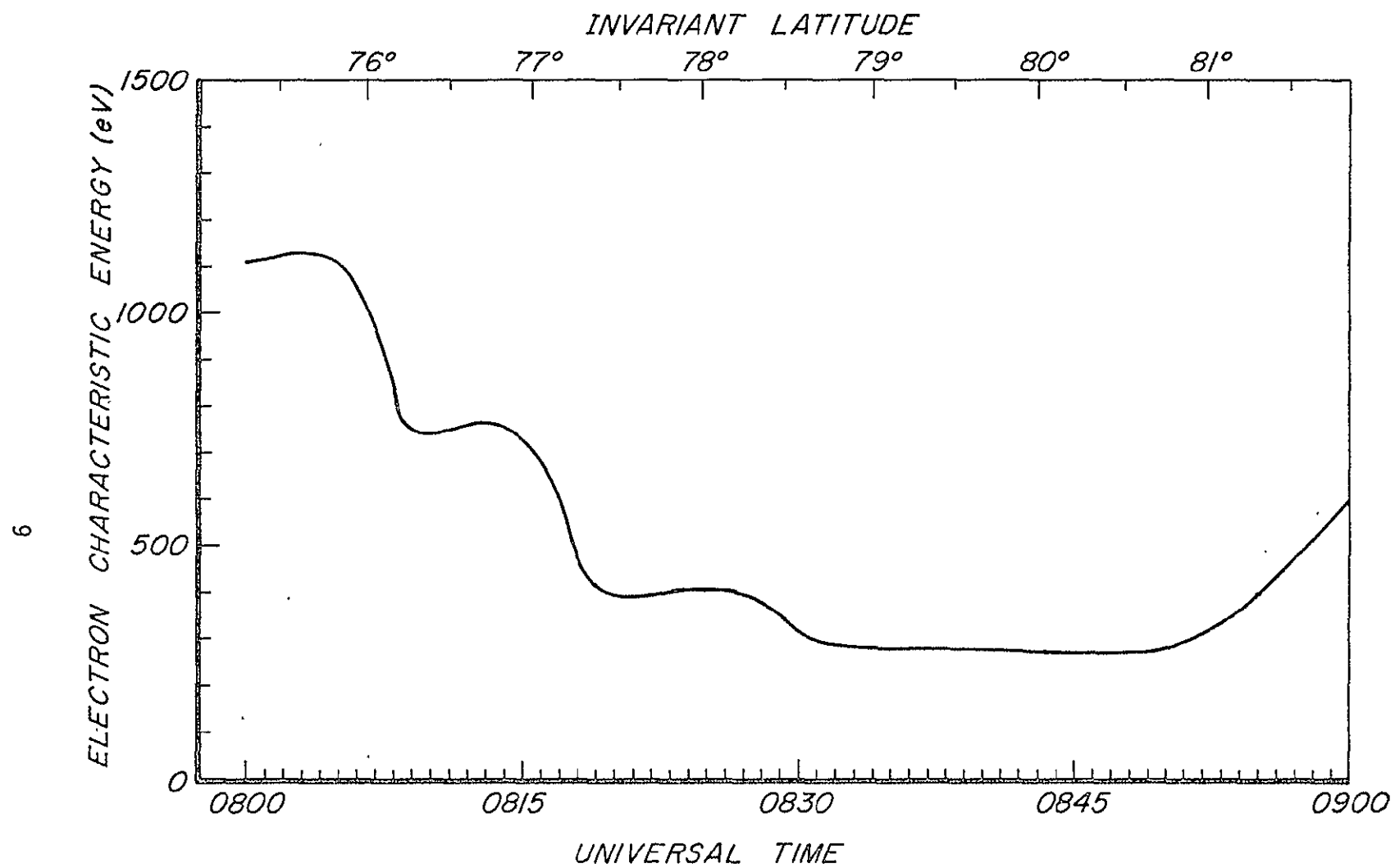


Figure 3

- (1) Cusp: $78^\circ < IL < 81^\circ$. Proton precipitation. Also precipitation of electrons with characteristic energy ~ 250 eV.
- (2) $76.5^\circ < IL < 78^\circ$. Electrons with characteristic energy of ~ 700 eV precipitating.
- (3) South of IL 76.6° . No protons. Precipitation of electrons with characteristic energy ~ 1.1 kev.

Both the latitudinal distribution of electrons and their characteristic energies, as well as the location and extent of proton precipitation zone, around local magnetic noon during magnetically quiet conditions, derived from photometric measurements agree with ISIS particle measurements (Winningham, 1971). Detailed comparison with the results from ESRO IA particle measurements are presented below.

D. COMPARISON OF RESULTS FROM ESRO IA PARTICLE MEASUREMENTS WITH CV 990 PHOTOMETRIC OBSERVATIONS

Figure 4 shows the track of ESRO IA satellite and the flight path of CV 990 on December 13, 1969. Experiments aboard these two vehicles were monitoring the aurora from the same region in most parts of the mid-day oval; e.g., at UT 0827 both the CV 990 aircraft and the ESRO IA satellite were at IL 78° at their respective flight and orbit altitudes, and both the photometric and particle measurements were made simultaneously along the same magnetic meridian. Both particle and photometric measurements point to magnetosheath protons precipitating north of the last closed geomagnetic field line. The latter is indicated by an abrupt decrease in kev electron flux and 4278 intensity around IL 78° . The spatial extent of the cusp appears to be covered by low energy magnetosheath-proton precipitation giving rise to weak H_β emissions.

We first compare the satellite proton measurements with airborne H_β measurements. Figure 5 shows the latitudinal variation in H_β intensity

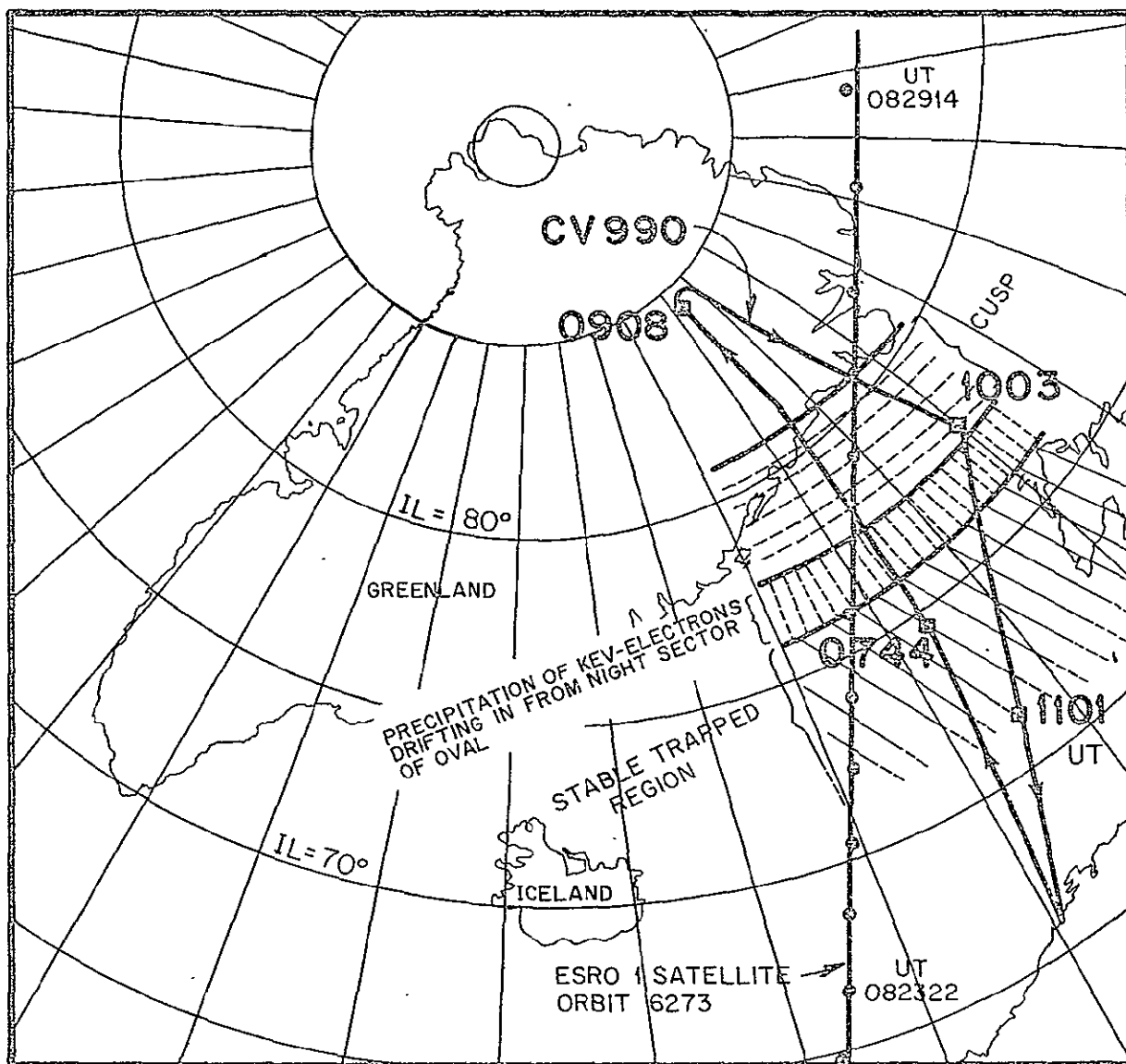


Figure 4

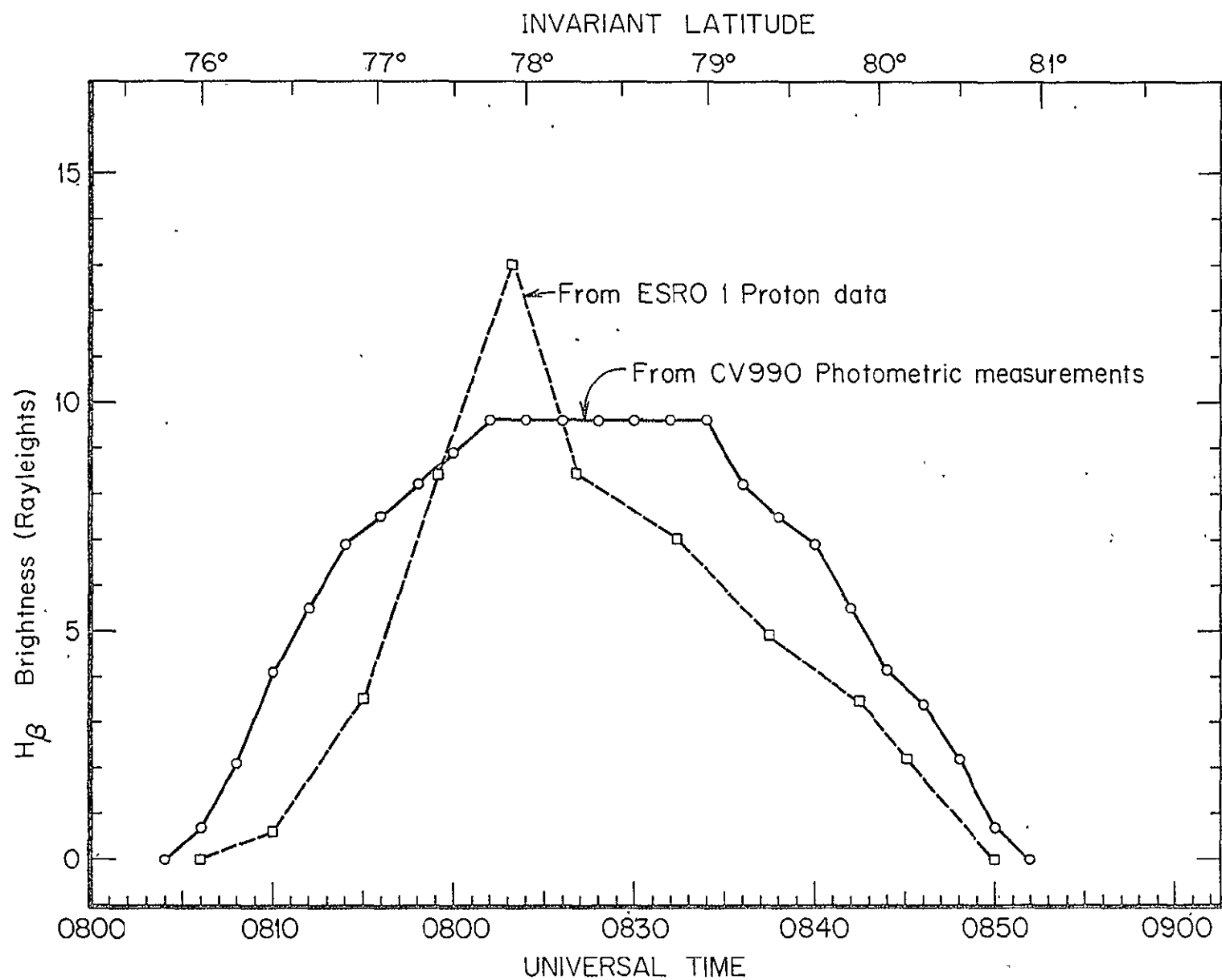


Figure 5

calculated from ESRO IA measurements of magnetosheath protons and McNeal and Birely's (1973) cross-sections for the production of H_{β} (Sivjee and Rees, 1975). The photometrically measured spatial variation in H_{β} intensity is also shown in the same figure. While the good agreement between the calculated and observed H_{β} intensity values is aeronomically interesting, the most important observation, in defining magnetospheric boundaries, is that the two track each other very well. The slightly broader extent of photometrically detected H_{β} emission is due to spatial diffusion of neutral hydrogen atoms, formed from precipitating protons by charge exchange with atmospheric constituents, across geomagnetic field lines. Consequently, the photometric measurement of H_{β} in the mid-day auroras provides a good indication of the spatial extent of magnetosheath protons precipitating along the cleft. Hence, as long as H_{β} emission in the cusp region is separated from that produced by relatively higher energy protons, which may precipitate around the mid-sector of the oval, its spatial extent can provide an authentic mapping of the cusp. Additionally, photometric measurements of the OI 6300 and 5577, as well as N_2^+ 1NG 4278 emissions, together provide both a sensitive tool for mapping the cusp region as well as an assessment of the characteristic energy of the precipitating electrons.

The ESRO IA particle data are averaged over 0.5° in IL. The data shown in Figure 1 do not provide detailed information about the boundary between the cusp and the region south of it where electrons, injected on the nightside of the oval and drifting to the noon sector, precipitate. On the other hand, the photometric data identify this boundary as a broad region lying between IL 76.5° and 78° ; it is characterized by

precipitation of electrons peaked at 700 eV. The photometric measurements show 1.1 keV electrons precipitating south of IL 76.5° compared to the value of IL 77.5° for the poleward boundary of this zone surmized from the ESRO IA particle data. Photometric measurements prior to UT 0800 (not shown in Figure 2) place the equatorward edge of this keV-electrons precipitation zone (and the poleward edge of the stable trapped region) at approximately IL 70°. Projections of magnetospheric boundaries on the ionosphere derived independently from particle and photometric data are marked on an invariant latitude grid in Figure 4.

E. CONCLUSION

Photometric measurements of OI 6300 and N_2^+ 4278, or OI 6300 and 5577 emissions in the magnetic noon sector of the oval are adequate in mapping the cusp region. The first set of measurements provides additional data on characteristic energy of precipitating electrons, while an order of magnitude change in the $I(6300)/I(5577)$ ratio (from about 0.4 to greater than 4) is a more dramatic indication of the transition from quasi-trapped to cusp region. Measurements of H_β emission can be used in mapping the cusp region as long as they are unambiguously separated from hydrogen emissions produced by relatively more energetic protons precipitating equatorward of the oval. There is a definite advantage in monitoring all four emissions; information relating to both precipitating electrons and protons, as well as corroborative evidence and hence a check on the former, can be derived from them.

In conclusion, the photometric measurements appear to be sensitive enough to map the trapping zone, the particle precipitation zone equatorward of the cusp and the cusp region where magnetosheath particles precipitate around the mid-day sector of the auroral oval.

II. OPTICAL EMISSIONS FROM THE MID-DAY AURORA

A. INTRODUCTION

According to satellite measurements, the ionosphere in the mid-day auroral region is bombarded by low energy electrons and protons (Winningham, 1972; Gladyshev et al., 1974). The study of optical emissions produced by the interaction of these particles with atmospheric constituents in the auroral region have so far been limited only to a few line and band emissions (Eather and Mende, 1971; Peterson and Shepherd, 1974; Sivjee and Hultqvist, 1975). It is shown here that detailed spectroscopic studies of mid-day auroral optical emissions have the potential of providing information on various phenomena including the interactions between low energy protons, hydrogen atoms and electrons with the atmosphere, vibrational distribution of $N_2^+(B^2\Sigma_g^+)$ produced by such interactions, resonant scattering of sunlight by N_2^+ and He (2^3S), and He abundance in polar regions relative to mid-latitudes. Intensities of various optical emissions from mid-day auroras and spectral profile of N_2^+ ING bands measured aboard NASA's Convair 990 jet aircraft are presented. These are compared with simple calculations based on our present knowledge of the types and energy distributions of particles precipitating in the mid-day auroral region and the available cross-sections for the excitation of various optical emissions in air.

B. EXPERIMENTAL

Measurements of optical emissions from mid-day aurora were made with a half-meter Ebert scanning spectrophotometer and several tilting as well as fixed position interference filter photometers (Sivjee,

1973). The spectrometer, operating at 5 Å resolution, scanned the wavelength interval from 3100 to 4000 Å, a range that includes auroral emissions from N_2^+ 1NG bands and He. Intensities of atomic emissions, at 5577 and 6300 Å from OI, 5200 Å from NI and 4861 Å from hydrogen, and molecular emissions, from N_2 2P (0,0) band at 3371 Å and N_2^+ 1NG (0,1) band at 4278 Å, were measured with a multichannel photometer (Dick et al., 1971) and a four channel tilting filter photometer (Eather and Mende, 1971). All these instruments were located in the Convair 990 below 65° elevation windows and oriented to view essentially vertically upward. The fields of view of the spectrometer and of the multichannel photometer were 10° whereas the tilting filter photometer had a 3° full angle field.

The measurements were made during the 1969 Auroral Airborne Expedition on a flight that originated in Bodo, Norway, on 13 December 1969 UT, for observation of the mid-day aurora. These aurorae are associated with the cleft region where magnetosheath particles have direct access to the ionosphere. The flight path and the time are shown in Figure 6. Also shown is a track of the ESRO IA satellite for the time interval in which the airborne measurements were made. Aurorae encountered in the mid-day section of the oval were mostly red patches; an example, obtained with the all sky camera on board the aircraft at UT 0839 has been published by Heikkila et al. (1972). The red character of the aurora is borne out by the photometric measurements of $\lambda 6300$; the emission exceeded a kilorayleigh during one brief interval. The time history (or the spatial variation) of some of the photometrically observed emission features, presented in Figure 7, shows that poleward of 77.5° the

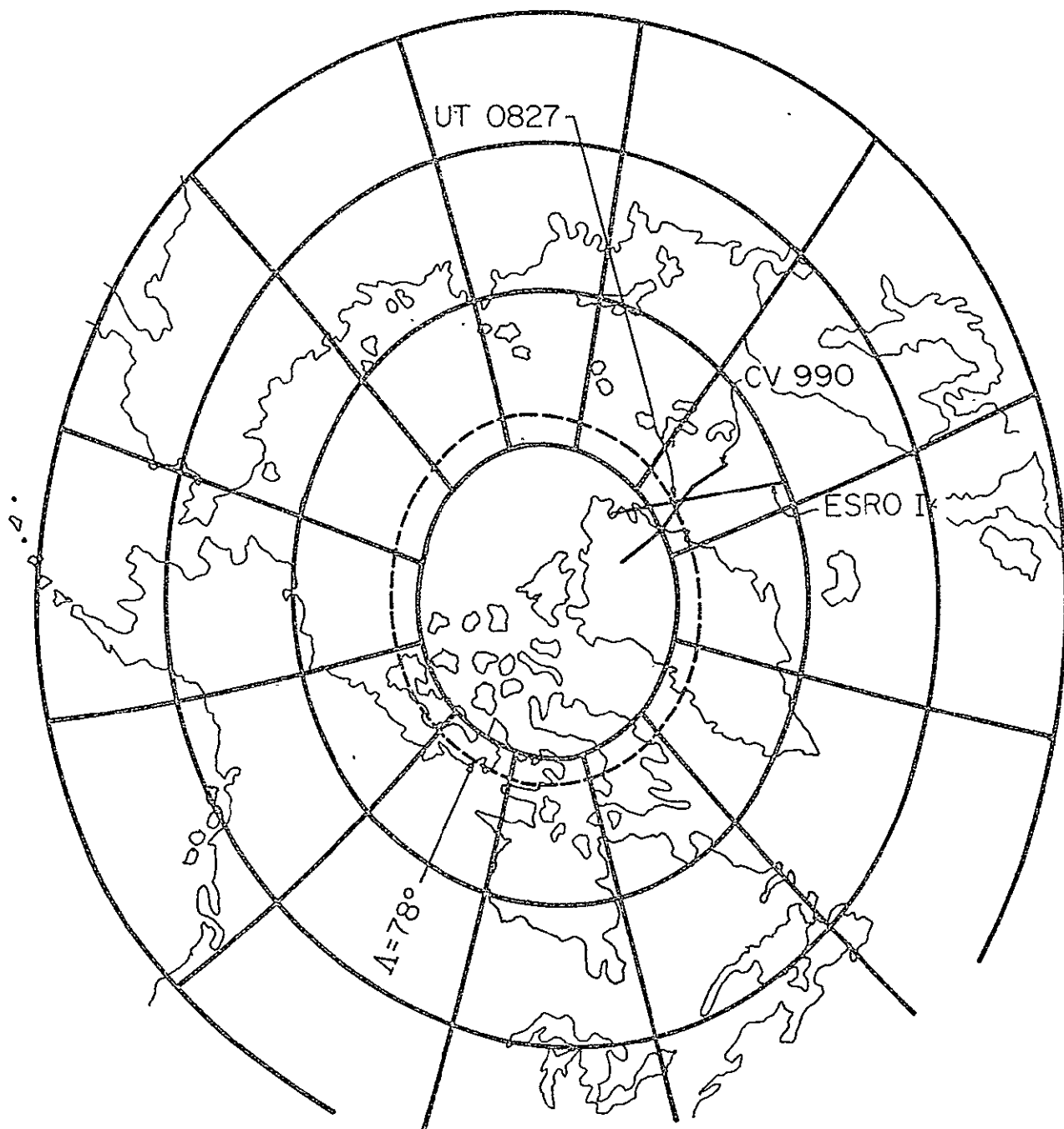


Figure 6

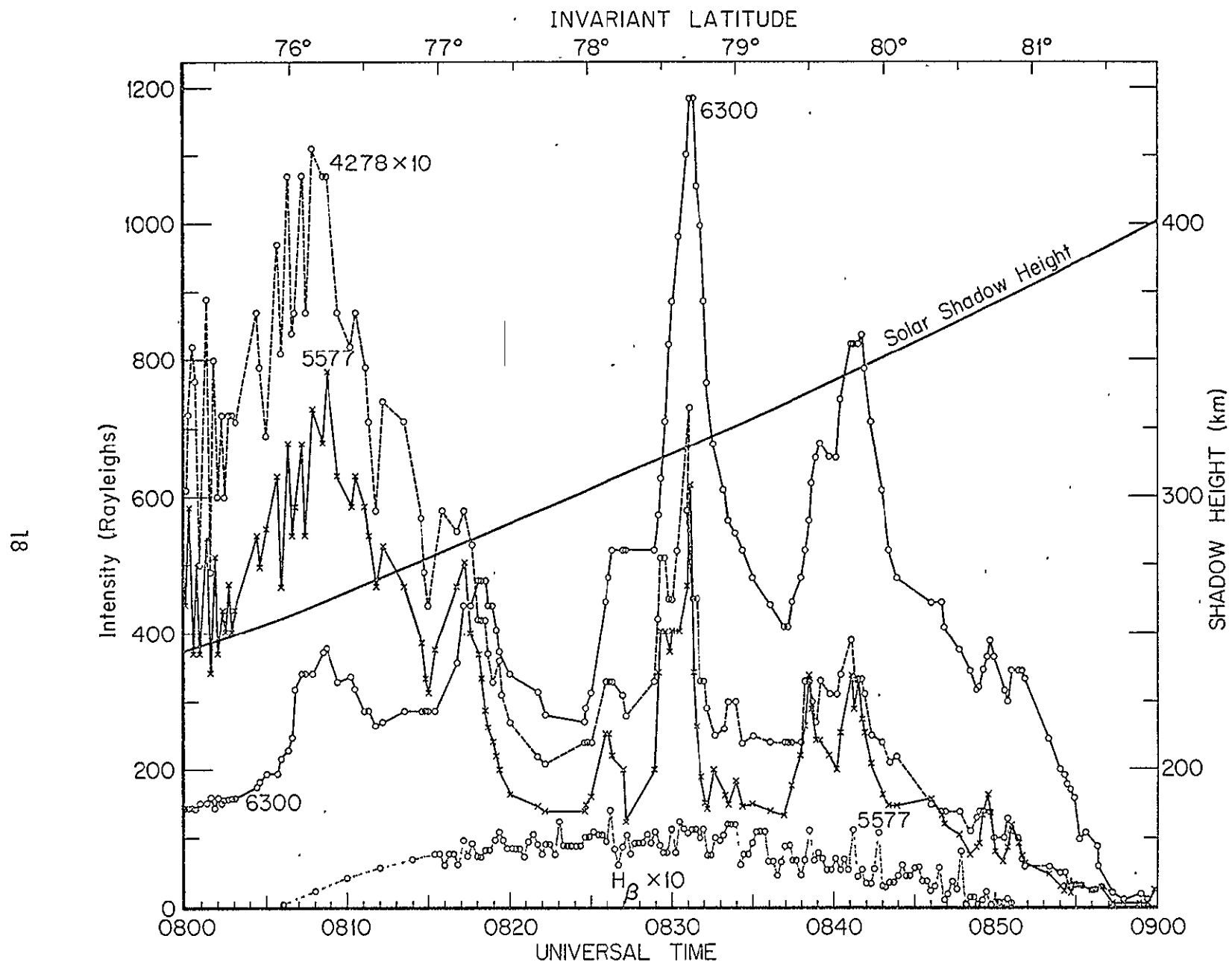


Figure 7

ratio $I(6300)/I(5577)$ exceeded unity by a substantial amount. A sum of 18 individual, 100 second spectrophotometer scans obtained during the period 0820 to 0850 UT is shown in Figure 8. The striking feature of this spectrum, compared to nighttime auroral observations, is the high intensity of the emissions around 3886 Å relative to the N_2^+ 1NG (0,0) band. This is more clearly illustrated in Figure 9 which shows the spectral region between 3870 and 3920 Å. High rotational development of the N_2^+ 1NG (0,0) band and large ratio of the emissions around 3886 Å to N_2^+ 1NG (0,0) band intensity are the interesting features. The apparent absorption features around 3893, 3898 and 3903 are similar to those observed by Brandt et al. (1965) and may represent Swing's effect.

The observed photon emission rates of the mid-day auroral spectroscopic features, averaged between 0820 and 0850 UT, are listed in Table I.

TABLE I

Spectroscopic Feature	Emission Rate (R)
O I ($\lambda 6300$)	520
O I ($\lambda 5577$)	183
N_2^+ 1NG (0,1) ($\lambda 4278$)	26
N_2 2PG (0,0) ($\lambda 3371$)	32
H Balmer β	7
NI (5200)	11

The electron and proton measurements on the ESRO IA satellite in the mid-day auroral region on December 13, 1969 UT showed large flux of low energy protons poleward of 77° coinciding with about two orders of magnitude decrease in the 1.3 keV electron flux (Sivjee and Hultqvist,

Figure 8

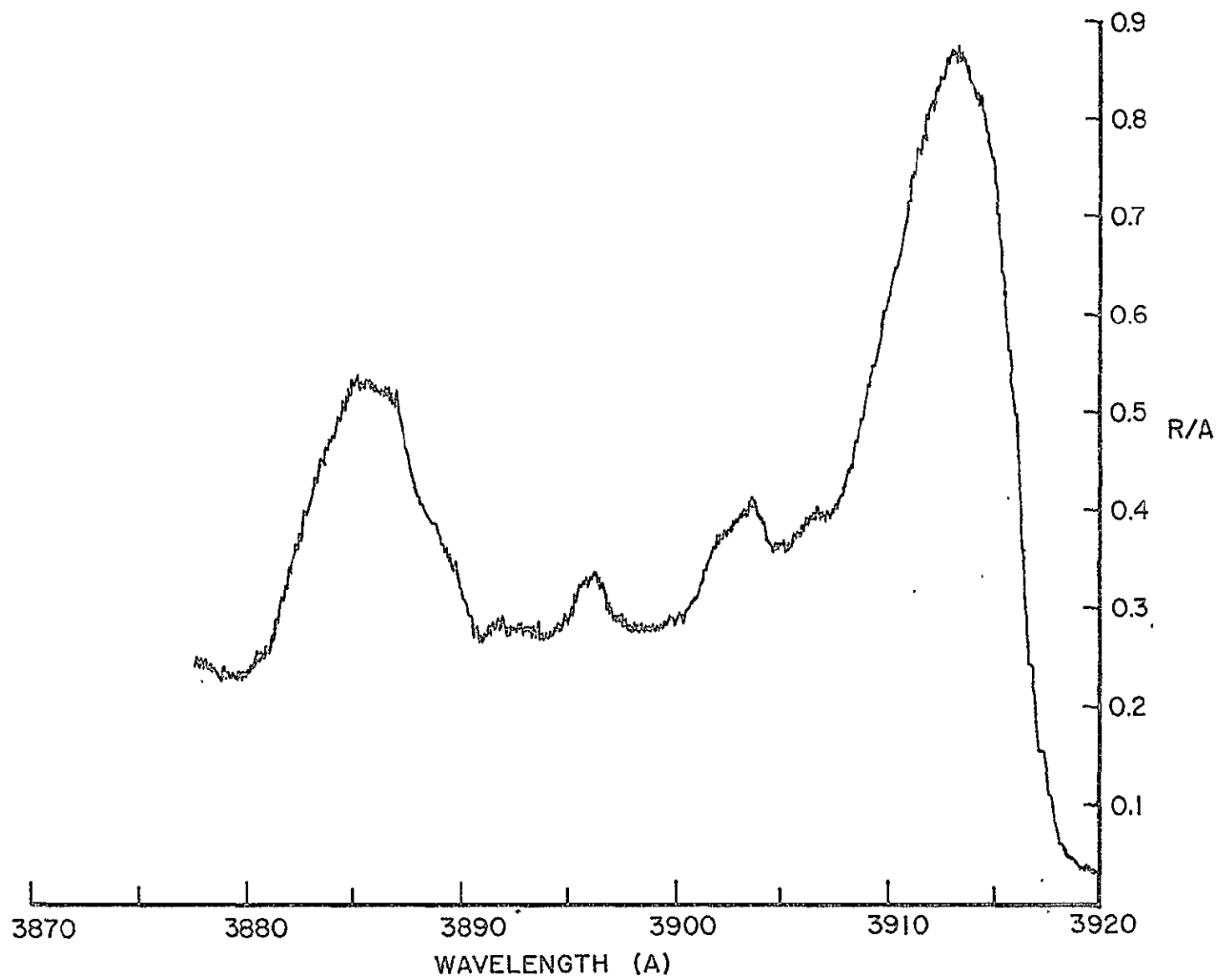


Figure 9

1975). The maximum in the proton flux occurred at about 0827 UT at 78° invariant latitude (IL); the aircraft crossed this latitude at the same time. The average precipitating flux of 1.4 and 6.3 keV protons observed on ESRO IA in the cusp region were 2.5×10^7 and 4.5×10^4 protons-(cm² sec sterad keV)⁻¹ (Sivjee and Hultqvist, 1975).

Magnetic activity during the midday auroral observation period was at a low level, the K_p index varying between 0 and 1.

C. ANALYSIS

Winningham (1972) and Gladyshev et al. (1974) have shown that low energy protons and electrons precipitate in the cusp region. Photometric measurements shown in Figure 2 and corresponding particle data from ESRO IA satellite (Sivjee and Hultqvist, 1975) lead to the same conclusion for the local magnetic noon sector of the auroral oval on December 13, 1969 for the period UT 0820 to 0850. Consequently, the excitation of atmospheric constituents by low energy protons and electrons are possible mechanisms for the production of the observed optical emissions in mid-day aurora. These processes are considered in estimating the intensities of various optical emissions from the mid-day aurora. Additionally, because of the relatively low solar shadow height (290 to 370 km) and the presence of absorption features in N₂⁺ 1NG (0,0) band profile which may represent Swing's effect, the contribution of solar resonance scattering by N₂⁺ to the intensity of auroral N₂⁺ 1NG (0,1) band is also derived. The emissions around 3886 Å are discussed in the last part of this section.

1. Interaction of Magnetosheath Protons with the Atmosphere

Satellite particle measurements by Winningham (1972) and Gladyshev et al. (1974) suggest that during magnetically quiet conditions the energy distribution of precipitating cusp protons can be approximated by a Maxwellian form with average energy of about 1 kev:

$$\frac{dN(E)}{dE} = A E e^{-E/\alpha} \quad (1)$$

According to ESRO IA measurements, the average flux of 1.4 and 6.3 kev protons, precipitating in the cusp region during the period of optical observations reported here, fit Equation (1) for $\alpha = 0.63$ kev (average energy = $2\alpha = 1.26$ kev) and $A = 1.67 \times 10^8$ protons-(cm² sec sterad kev²)⁻¹. Hence, about 2.1×10^8 protons-(cm² sec)⁻¹ carrying 0.42 ergs-(cm² sec)⁻¹ were released into the mid-day ionosphere in the region $78^\circ \leq IL \leq 81^\circ$.

The excitation rate of atmospheric species X can be calculated from the relation

$$\eta(X^*) = \int_0^\infty n(X,h) \int_{E_1}^\infty \sigma(X,E) \frac{dN(E,h)}{dE} dEdh, \quad (2)$$

where $n(X,h)$ is the density of X at height h, $\sigma(X,E)$ the excitation cross-section and E_1 the threshold energy for exciting X to a particular state. Practical application of (2) is limited by the lack of proton energy spectra at all heights and dearth of $\sigma(X,E)$ at proton energies below a few kev (McNeal and Birely, 1973; Birely, 1974). Hence, only rough estimates of excitation rates can be made.

Assuming that the ionization and excitation effects of cusp protons in air are equivalent to that of a monoenergetic (1.3 kev) flux, N_p ,

of 2.1×10^8 protons-($\text{cm}^2 \text{ sec})^{-1}$, we can estimate the intensities, $I(X, \lambda)$, of various optical emissions, at wavelength λ , from the mid-day aurora.

$$I(X, \lambda) = n(X) N_p(E) \sigma(E, X, \lambda) A(X, \lambda) \tau \quad (3)$$

Here $n(X)$ is column density of X above the stopping height of protons with energy E , A the transition probability and τ the effective lifetime of the emitting level. To determine $n(X)$ we note that the residual range of 1 kev protons is 0.0038 atm-cm (Eather, 1967) which in a Jacchia (1965) model atmosphere, appropriate for the mid-day aurora considered here, is about 161 km. Now, 1 kev protons attain a charge-equilibrated state of 95% hydrogen atoms (H) and 5% protons (H^+) after only a few collisions with air particles (McNeal and Birely, 1973). Thus, ionization and excitation of atmospheric constituents during precipitation of protons with energy around 1 kev are produced almost entirely by such a charge-equilibrated beam at all heights above 161 km. Using Birely's (1974) cross-section for the excitation of $N_2^+(B^2\Sigma_u^+, v'=0)$ by 1.3 kev H and H^+ , Shemansky and Broadfoot's (1971) transition probabilities and a column density of $6 \times 10^{16} \text{ cm}^{-2}$ for N_2 above 161 km we get:

$$\begin{aligned} I(4278) &= 6 \times 10^{16} \times 2.1 \times 10^8 \times (0.05 \times 1.78 + 0.95 \\ &\quad \times 0.19) \times 10^{-17} \times 3.35 \times 10^6 \times 6.58 \times 10^{-8} \\ &\quad \text{photons } (\text{cm}^2 \text{ sec})^{-1} \\ &\approx 8 \text{ R.} \end{aligned}$$

Hence, for protons with energies around 1 kev, $I(4278)/I(H\beta) \approx 1.1$ or $I(3914)/I(H\beta) \approx 3.7$. The latter may be compared with a value of 7

derived by Eather (1967) for 1 kev protons, and between 10 and 17.5 observed by Eather (1968) in nighttime auroras where precipitating protons generally have much higher (~ 10 kev) energy.

The intensity of N_2 2P(0,0) band can be similarly estimated using Birely's (1974) cross-section for excitation of $N_2(C^3\pi_u^+)$ by 1.3 kev H and the ratio of 3371 intensity to total N_2 2P band-system intensity (Vallance Jones, 1971):

$$I(3371) = 6 \times 10^{16} \times 2.1 \times 10^8 \times 4.5 \times 10^{-18} \\ \times 0.244 \text{ photons} \cdot (\text{cm}^2 \text{ sec})^{-1} \approx 14 \text{ R.}$$

The effective cross-sections, $\sigma_{\text{eff}}(H\beta)$, for $H\beta$ production involves cross-sections for the excitation of three different levels and none of them have been measured for 1.3 kev protons. Hence, it is best to derive $\sigma_{\text{eff}}(H\beta)$ from our $H\beta$ intensity and proton flux measurements rather than extrapolating the high energy cross-section values to calculate $I(H\beta)$:

$$\sigma_{\text{eff}}(H\beta) = \frac{7 \times 10^6}{6 \times 10^{16} \times 2.1 \times 10^8} \text{ cm}^2 \\ \approx 6 \times 10^{-19} \text{ cm}^2.$$

The OI red and green line emissions are mostly excited by very low energy (< 100 eV) electrons. Lack of differential cross-sections for secondary electron production by H and H^+ collisions in air precludes direct assessment of the proton component of 6300 and 5577 intensities. A rough estimate based on Eather's (1968) measurements, pertaining mostly to high energy protons, indicates that very little of the OI red emission in the cusp is excited by magnetosheath protons.

From the above discussions, it is apparent that protons precipitating in the cusp region will not account for all N_2^+ , N_2 and OI emissions. This conclusion is reinforced by the observed variations in optical emissions from the cusp (see Figure 7). Since the H β intensity, indicative of proton flux, is fairly steady while the N_2^+ , N_2 and OI emissions are highly structured, one cannot attribute all the observed optical emissions to proton excitation of air particles. Detailed correlations among the variations in N_2^+ , N_2 and OI emissions point to a common excitation source for at least part of these emissions.

2. Electron Interaction with the Atmosphere

From several hundred cusp electron spectra monitored on ISIS I satellite, Winningham (1971) showed that the flux of magnetosheath electrons peak at energies between 100 and 300 eV in at least 75% of these measurements. Intensity ratios of cusp optical emissions shown in Figure 2 also point to the precipitation of soft (~ 500 eV average energy) electrons (Sivjee and Hultqvist, 1975). To calculate the intensities of optical emissions resulting from the interaction of these soft magnetosheath electrons with the atmosphere we need to know, in addition to the average energy of these electrons, their total flux. This information can be derived from 4278 intensity measurement after correcting it for contribution from proton excitation (~ 8 R, see previous section) and resonant scattering of sunlight by N_2^+ ions. The following iterative procedure was employed in determining the fraction of measured 4278 intensity excited solely by magnetosheath electrons. First, an ionization profile required to produce 18 R of 4278 by electron impact on N_2 was determined from Banks et al.'s (1974) calculations for electrons

with average energy of 420 eV which is approximately equal to that of cusp electrons for the period UT 0820-0830 on December 13, 1969. From this information the equilibrium density distribution of N_2^+ ions (Feldman, 1973) was derived. Using a g factor of 0.013 (Broadfoot, 1967), the intensity of resonantly scattered sunlight at 4278 was calculated. To this was added the corresponding value determined from proton induced ionization and the sum was subtracted from 18 R. The above procedure was repeated using the net 4278 intensity as the starting value. After several iteration the intensity of electron excited 4278 was determined to be 13 R which implies a total electron number flux of 1.68×10^8 electrons-($\text{cm}^2 \text{ sec}$)⁻¹ depositing about 0.13 ergs ($\text{cm}^2 \text{ sec}$)⁻¹ in the atmosphere.

Banks et al. (1971) have calculated the 6300 emission resulting from precipitation of 420 eV electrons. When normalized to correspond to precipitating flux of 1.68×10^8 electrons, their calculations yield an intensity of 545 R of 6300 emission. Calculation of electron excited 5577 intensity, based on Bank et al.'s (1974) secondary electron spectra for 420 eV primaries and Henry et al.'s (1969) excitation cross-section, yields 136 R. To calculate the intensity of electron excited 3371 band emission we used an established relation between 3371 and 4278. Both auroral observation (Rees et al., 1975) and theoretical calculations (Rees and Jones, 1973) yield 0.84 for $I(4278)/I(3371)$ and this ratio should be independent of electron energy, at least for primary electrons with energies greater than about 100 eV. Consequently, 13 R of 4278 imply 16 R of electron excited 3371 from the mid-day aurora of December 13, 1969. No reliable measurements of the parameters which enter in

computation of NI(5200 Å) intensity are available. It is therefore not feasible to predict the intensity of this auroral emission.

Table II summarizes the predicted intensities of electron excited optical emissions from mid-day aurora. Comparing these values with observations, listed in Table I, we find that most of the OI emissions and about half of the N_2^+ and N_2 emissions from the mid-day aurora are excited by electrons.

TABLE II

Predicted Intensities of Optical Emissions Excited
by Magnetosheath Electrons in the Cusp Region

Emission (Å)	Intensity (R)
4278	13
6300	545
5577	136
3371	16

3. Resonant Scattering of Sunlight by N_2^+ Ions

The intensity of resonantly scattered sunlight at 4278 Å in the mid-day aurora was determined from the equilibrium density profile of N_2^+ and using a g-factor of 0.013. The former was derived from the altitude profile of total ionization based on Banks et al.'s (1974) calculations for 420 eV electrons and the total ionization cross-sections for 1.3 keV protons compiled by McNeal and Birely (1973). These calculations place upper limits of 4 and 1 R for the intensities of sunlight at 4278 scattered by N_2^+ ions formed through electron and proton interactions with the atmosphere. Hence, less than 20% of the 4278 intensity measured in the mid-day aurora came from resonantly scattered sunlight.

This conclusion is confirmed by detailed correlation between 4278 and 3371 intensities observed in the mid-day aurora.

4. Auroral Emissions Around 3886 Å

There are two candidates for the mid-day auroral emissions observed around 3886 Å: N_2^+ 1NG (1,1) band at 3884 Å and He ($3^3P \rightarrow 2^3S$) at 3888 Å. The former may seem a weak candidate since in nighttime electron excited auroras the ratio of N_2^+ 1NG (1,1) to (0,0) band is normally about 1 to 24, much smaller than the ratio of the feature around 3886 Å to N_2^+ 1NG (0,0) band shown in Figure 9. Moreover, the rotational distribution of N_2^+ ($B^2\Sigma_g^+$) in nighttime auroras is normally thermalized while a rotational temperature of about 2000°K is deduced from mid-day auroral measurements (see Figure 10). However, the presence of low energy protons in the cusp region may produce a vibrational distribution of N_2^+ 1NG bands which is not proportional to population weighted Franck Condon factors and a rotational distribution with characteristic temperature much higher than ambient kinetic temperature (Moore and Doering, 1969). Additionally, about 20% of the observed N_2^+ 1NG band emission was produced by resonant scattering of sunlight, a process which also leads to an apparent abnormal vibrational and rotational distribution of N_2^+ 1NG bands (Vallance-Jones and Hunten, 1960; Broadfoot and Hunten, 1966). Hence, these two processes as well as the impact of low energy electrons on N_2 (Walker et al., 1969) must be considered to determine the ratio of N_2^+ 1NG (1,1) to (0,0) bands in mid-day aurora.

Assuming for the moment that the feature around 3886 Å represents N_2^+ 1NG (1,1) band, we can determine the vibrational and rotational distributions of N_2^+ ($B^2\Sigma_u^+$), required to produce the observed ratio of N_2^+

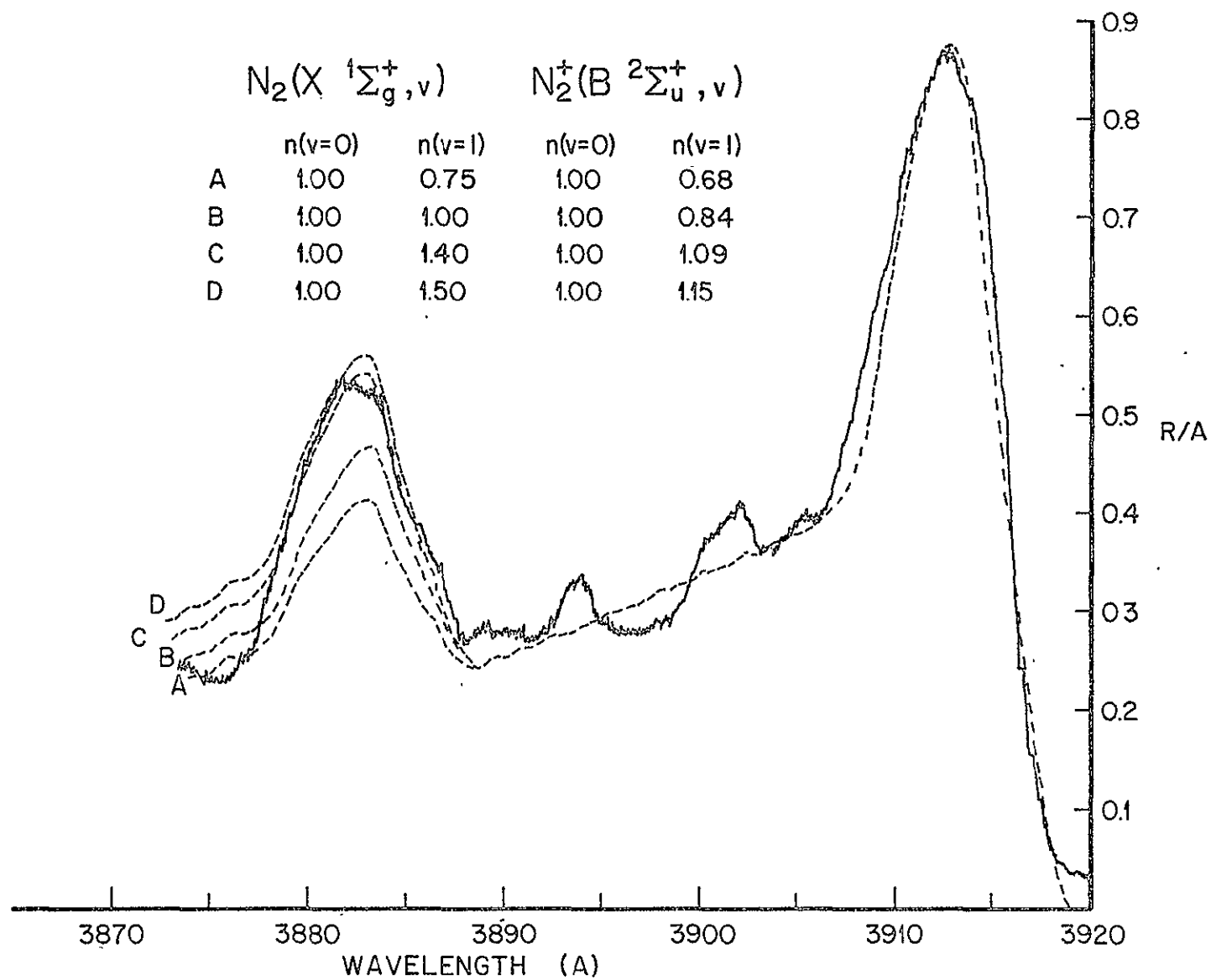


Figure 10

1NG (0,0) to (1,1) band intensities, by constructing various synthetic profiles of these bands for comparison with observation. The synthetic profiles of N_2^+ 1NG bands shown in Figure 10 depend on three parameters: (1) the rotational distribution of $N_2^+(B^2\Sigma_u^+, v)$, (2) the relative populations of various vibrational levels of $N_2^+(B^2\Sigma_u^+)$, and (3) the relative transition probabilities of the bands (Shemansky and Broadfoot, 1971). We have assumed a Boltzmann distribution of the rotational levels characterized by a temperature $T_{ROT} = 2000^\circ K$ and have considered four different ratios of the populations of the zeroth and first vibrational levels. Synthetic profiles of N_2^+ 1NG (0,0) and (1,1) bands for the case when the instrumental half-width of each rotational line is 5 Å are shown in Figure 10 together with our observations from midday aurora. If we assume, as is done in Figure 10, that the unidentified feature represents the N_2^+ 1NG (1,1) band then the best fit between synthetic and observed spectral profiles exists for the case in which the population of the zeroth and first vibrational levels of $N_2^+(B^2\Sigma_u^+)$ are in the ratio of 1 to 1.15. A possible mechanism for producing such a vibrational distribution of $N_2^+(B^2\Sigma_u^+)$ is the impact of low energy H^+/H on N_2 .

As pointed out earlier, about 95% of a 1 keV charge-equilibrated beam consists of neutral hydrogen atoms. Hence, simultaneous ionization and excitation of N_2 by H is important for the production of N_2^+ 1NG band emissions from mid-day aurora. According to Birely (1974), the ratios of H excited N_2^+ 1NG band emissions originating from different vibrational levels increasingly deviate from the ratios of population weighted Franck-Condon factors. For proton impact the effect is similar but not as pronounced as for atomic hydrogen (Moore and Doering, 1969). In both

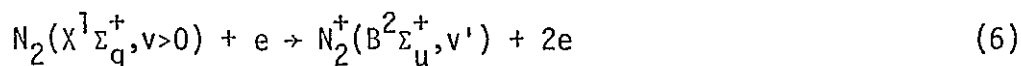
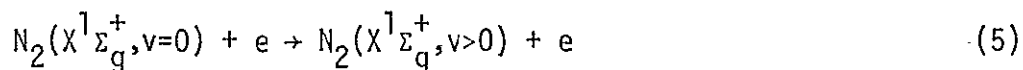
cases the rotational distribution of $N_2^+(B^2\Sigma_u^+)$ is characterized by a Boltzmann temperature much higher than the kinetic temperature of ambient gas. To assess the relative populations of the zeroth and first vibrational levels of $N_2^+(B^2\Sigma_u^+)$ produced by the impact of 1.3 keV H on N_2 we extrapolate Birely's (1974) excitation cross-sections to lower energies and employ Shemansky and Broadfoot's (1971) transition probabilities:

$$\frac{N_{v'=0}}{N_{v'=1}} = \frac{\sigma(1,2) A_{0,1}}{A_{1,2} \sigma(0,1)} \approx 3.7 \quad (4)$$

which is much smaller than the population inversion required to identify the feature around 3886 Å as N_2^+ ING (1,1) band. The difference between the observed intensity of the emission around 3886 Å and the intensity of N_2^+ ING (1,1) band calculated from synthetic profile of the band for the case when $N_{v'=0}/N_{v'=1} = 3.7$, and for rotational temperature of 2000°K, works out to 11 R.

Clearly, hydrogen impact of an N_2 will not explain the observations since an inverted vibrational population of $N_2^+(B^2\Sigma_u^+)$ is required if all the observed emissions at 3886 Å come from H excited N_2^+ ING (1,1) band. Such an inverted vibrational population of $N_2^+(B^2\Sigma_u^+)$ is not suggested by the relative intensity of N_2^+ ING (1,0) band at 3582 Å (see Figure 8).

An alternative excitation mechanism, which may produce a higher ratio of N_2^+ ING (1,1) to (0,0) band intensities than normally observed in bright nighttime auroras, is the vibrational excitation of N_2 by low energy electrons followed by electron ionization and excitation of these species (Walker et al., 1969):



To determine the effect of this mechanism in mid-day auroras we first assess the vibrational distribution of $N_2(X^1\Sigma_g^+, v)$ required to produce the observed ratio of N_2^+ ING (0,0) to (1,1) band intensities.

In electron excitation of N_2^+ ING bands the Franck Condon mechanism does apply for all electron energies. We have calculated the vibrational distribution of $N_2(X^1\Sigma_g^+, v)$ that would give rise to various vibrational distributions of $N_2^+(B^2\Sigma_u^+)$, using Nicholls' (1962) ionization Franck Condon factors and Shemansky and Broadfoot's (1971) transition probabilities. In Figure 10 the correspondence between the populations of $N_2(X^1\Sigma_g^+)$ and $N_2^+(B^2\Sigma_u^+)$ vibrational states is shown for the case of electron excitation. To produce the emission observed around 3886 by electron impact on N_2 would require ground state N_2 molecules to be distributed between the zeroth and first vibrational levels in the ratio of 1 to 1.5. However, calculations of N_2 vibrational excitation by electrons and quenching by atomic oxygen shows that under steady state conditions only a small fraction of N_2 molecules in the mid-day aurora remain in vibrational levels higher than $v'=0$. It therefore appears unlikely that electron bombardment can cause a population inversion among the vibrational levels of $N_2(X^1\Sigma_g^+)$.

It was shown earlier that only about 20% of the N_2^+ ING band intensity observed in the mid-day aurora arises from resonant scattering of sunlight. However, even if we assume that resonant scattering of sunlight produces all the N_2^+ ING band emissions in mid-day aurora, the

difference between observations and synthetic band profile, drawn for the case $T_{VIB} = 2050^{\circ}\text{K}$, $T_{ROT} = 2000^{\circ}\text{K}$ (Vallance Jones and Hunten, 1960) and normalized to the measured intensity of $\text{N}_2^+ \text{ING (0,0)}$ band, amounts to about 10 R of excess emission around 3886 Å.

Clearly, neither particle impact on N_2 nor solar resonant scattering of sunlight would produce enough $\text{N}_2^+ \text{ING (1,1)}$ band photons to account for the total intensity of the emissions around 3886 Å observed in mid-day aurora. Considering all these excitation mechanisms we are still left with about $9 \text{ R} \pm 2 \text{ R}$ of unidentified optical emissions around 3886 Å to account for.

An alternative source of emission around 3886 Å is resonant scattering of sunlight by ortho He ($2^3\text{S}-3^3\text{P}$). According to Brandt et al. (1965) the intensity of He 3888 Å at mid-latitudes is less than 1 R. However, Christensen et al. (1971) have shown that the intensity of 10830 Å He ($2^3\text{S}-2^3\text{P}$) emission is a function of both the time of the year and of the solar cycle; its maximum zenith intensity in December 1969 for local solar depression angle of 15° was between 250 and 470 R excluding the contribution from conjugate photo electrons. The corresponding zenith intensity of 3888 Å emission should be between 2 and 3 R (Brandt et al., 1965). This is about a quarter to a third of the net intensity of the unidentified feature around 3886 Å observed in mid-day aurora ($78^{\circ} \leq \text{IL} \leq 81^{\circ}$) on December 13, 1969 UT when the local solar depression angle was between 16 and 19° .

Two phenomena may lead to higher He ($2^3\text{S}-3^3\text{P}$) 3888 Å emission at high latitudes. First, the polar winter bulge in He abundance (Keating and Prior, 1968; Keating et al., 1970) amounts to an increase of a

factor of three to four in the helium density over the winter pole thermosphere. This effect is more than adequate to produce 9 R of He 3888 Å emissions in mid-day auroral region. Hence, the emission feature around 3886 Å observed in mid-day aurora is most likely He 3888 Å blended with N_2^+ 1NG (1,1) band.

The precipitation of magnetosheath electrons (with energies greater than 20 eV) along the cleft could lead to higher fraction of He(2^3S) in mid-day aurora than at mid-latitudes where only photoelectrons can excite para He (1^1S) to ortho He (2^3S). However, during magnetically quiet conditions, the flux of 20 eV cusp electrons is typically about 6×10^6 electrons $(cm^2 \text{ sec eV})^{-1}$ (Winningham, 1972), much smaller than the photoelectron flux at 500 km used by Christensen et al. (1971) in their calculation of zenith intensity of ortho He emission. Since most of the He (2^3S) is formed above 400 km height the effect of magnetosheath electrons on He 3888 Å emissions may not be significant.

D. SUMMARY

In mid-day auroras about 30% of the N_2^+ 1NG and 45% of N_2 2P band emissions as well as 25% of OI green line emission may be produced through the interactions between magnetosheath protons and atmospheric constituents. Electrons precipitating in the cusp region account for almost all of the OI red and about three-quarters of the green emissions as well as 50% of N_2^+ 1NG and N_2 2P band emissions. Resonant scattering of sunlight by N_2^+ ions account for about 20% of N_2^+ 1NG band emissions from mid-day aurora. These optical measurements, coupled with various excitation cross-sections, show that the ratios of 4278, 3371 and 5577

to H β are approximately 1.1, 2.0 and 6.7, respectively, for 1.3 keV protons. The effective cross-section for H β emission from 1.3 keV protons precipitating in air works out to $6 \times 10^{-19} \text{ cm}^2$.

Resonant scattering of sunlight by He(2^3S) in polar regions of the northern hemisphere produces about 9 R of 3888 Å emission during magnetic noon in winter. Polar abundance of He(1^1S) in winter may be about three to four times higher than at mid-latitudes.

More extensive spectrophotometric observations of mid-day auroral optical emissions are needed at high enough resolution to separate He 3888 Å line from N $_2^+$ 1NG (1,1) band and to provide more definitive measurements of the vibrational and rotational distributions of the latter. Such studies have the potential of providing valuable information about interactions between air and low energy protons, hydrogen atoms and electrons as well as resonant scattering of sunlight by atmospheric constituents.

III. STUDIES OF MOLECULAR NITROGEN BANDS FROM AIRBORNE AURORAL SPECTROSCOPY

A. INTRODUCTION

Spectroscopic studies of auroral radiation have proven to be of great value in elucidating excitation processes of atomic and molecular species in the terrestrial atmosphere. Indeed, the low ambient density and absence of boundary walls in the upper atmosphere favor investigation of emission features from metastable states and chain reaction excitation processes that frequently cannot be investigated in the laboratory. On the other hand, energetic particle fluxes that produce the auroral radiations are highly variable in their location, energy distribution and flux magnitude. This variability introduces uncertainties when observations obtained from different aurorae or those averaged over a long time interval are used in quantitative studies of excitation processes.

One of the more sanguinary controversies in the auroral literature concerns the excitation of triplet states in molecular nitrogen that give rise to emission of the First Positive, Second Positive, and Vegard-Kaplan band systems (Shemansky and Broadfoot, 1973; Cartwright et al., 1973). The N_2 1PG bands radiate principally in the near infrared while the N_2 2PG and the N_2 V-K bands lie in the near and middle ultraviolet. To our knowledge, there have not been any previous spectrometric measurements made simultaneously in both spectral regions of a single auroral event; previous analyses have made use of auroral observations obtained at different times. During the 1969 Airborne Auroral Expedition aboard NASA's CV 990 aircraft, there was a brief period when two spectrophotometers,

having identical fields of view and look directions, monitored optical emissions from a westward traveling surge in the wavelength range 3100 to 4000 Å and 6200 to 6900 Å, respectively. Simultaneous observations of several bands of the 2PG, 1PG and V-K systems of N_2 were recorded. These measurements provide the most pertinent auroral data yet available that bear on the problem.

In addition to the N_2 bands enumerated above the near ultraviolet spectrum included a line due to a forbidden transition in atomic nitrogen and some allowed lines of OII and NII.

Absolute emission rates were obtained for all observed spectral features. This enables us to model quantitatively the auroral event and draw some conclusions regarding excitation mechanisms, excitation cross sections, and quenching rates.

B. INSTRUMENTATION AND CALIBRATION

Measurements were made by several instruments. A half-meter Ebert-Fastie spectrophotometer scanned the wavelength interval between 3100 and 4000 Å at 5 Å resolution in 25 seconds. The instrument is described in detail by Rees (1972). A one-meter Ebert-Fastie spectrophotometer, described by Dick et al. (1970), scanned the wavelength interval between 6200 and 6900 Å at a resolution of 15 Å with a scan period of 8 seconds. A multi-channel fixed filter photometer continuously monitored the N_2^+ 1NG (0,1) and (1,2) bands at 4278 and 4236 Å, the N_2 2PG (0,0) band at 3371 Å and the OI lines at 5577 Å and 6300 Å (Dick et al., 1971). A four-channel tilting filter photometer monitored the oxygen lines, the 4278 Å band, and the Balmer beta emission of atomic hydrogen (Eather and Mende, 1971). The spectrophotometers and the fixed filter photometers

had similar, though not identical fields of view, about 10° , while the tilting filter photometers had a 3° field of view. The instruments were mounted in the NASA Convair 990 aircraft directly under quartz windows in the top of the fuselage. With the aircraft in level flight the viewing direction was in the zenith.

The one-meter spectrometer and the multi-channel photometer were calibrated at the Johns Hopkins University using a tungsten-filament lamp as an optical source to illuminate a freshly coated MgO screen providing a uniformly bright Lambert surface. The tungsten-filament current, which could be controlled to better than one part in a thousand, was varied until the spectral brightness of the lamp matched that of another lamp calibrated by the National Bureau of Standards to run at an equivalent black-body temperature of 2508°K . An optical pyrometer was used to verify the match between the two lamps. The half meter spectrometer was calibrated at the University of Colorado using a quartz-iodide lamp which, in turn, was calibrated against a standard lamp by the procedure described above. A low light level source, consisting of fluorescent material deposited on a radioactive carbon base, was used for calibrating the tilting filter photometers, after having been calibrated against a standard lamp in the laboratory.

To check the consistency of the independent calibrations of the detectors a tungsten filament lamp and MgO screen were used to calibrate all the optical instruments on board the aircraft in the darkened hangar at Fort Churchill. The agreement among different experimental setups was within 15%. Coincident auroral observations on several flights generally yielded agreement within 15% in the measured brightness of

several emission features. Considering these variations, the accuracy of the measurements of the parameters which enter into the absolute calibrations (e.g., separation of lamp from screen, orientation of screen with respect to lamp, aperture size, transmission of lens, signal to noise ratio, etc.) and the uncertainty in the absolute brightness of the standard lamp we estimate a possible error in the absolute calibration of about 25%.

C. OBSERVATIONS

During the 1969 Auroral Airborne Expedition many different types of aurorae were encountered. However, simultaneous measurements of spectra in the UV and IR were recorded only for a brief period during a westward traveling surge observed on 26 November 1969. Although westward traveling surges usually exhibit large temporal and spatial fluctuations of intensity, it is possible to identify a brief period when the radiation, as viewed from the aircraft, was relatively steady. While not as bright as during the peak phase of the surge, the aurora is more suitable for analysis during the selected time interval 05:05:30 to 05:57:35 UT. An all-sky camera photograph of the aurora underflown by the aircraft is shown in Figure 11, with the field of view of the spectrometers superposed on the photograph. The aurora remained in the field of view of all the detectors from 05:54 to 06:00 UT. The time histories of the brightness of the 4278 Å band of N_2^+ and the OI lines at 5577 Å and 6300 Å recorded with the multichannel photometers are shown in Figure 12.

Single scans of the raw spectrophotometric measurements are shown in Figures 13 and 14. Figure 13 gives a spectral scan between 3100 Å and 4000 Å at a 5 Å resolution. The record from the magnetic tape is displayed

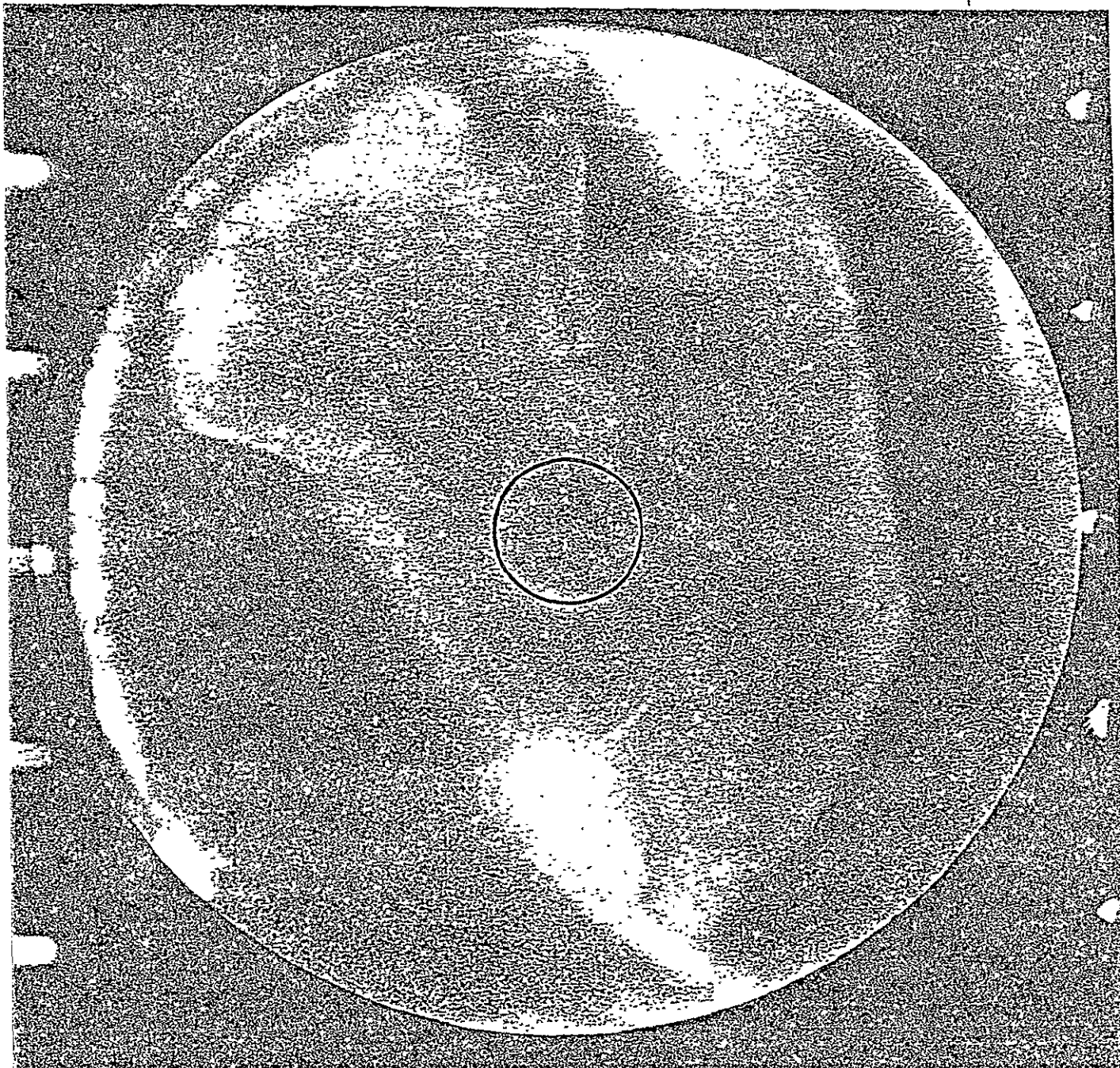


Figure 11

ORIGINAL PAGE IS
OF POOR QUALITY

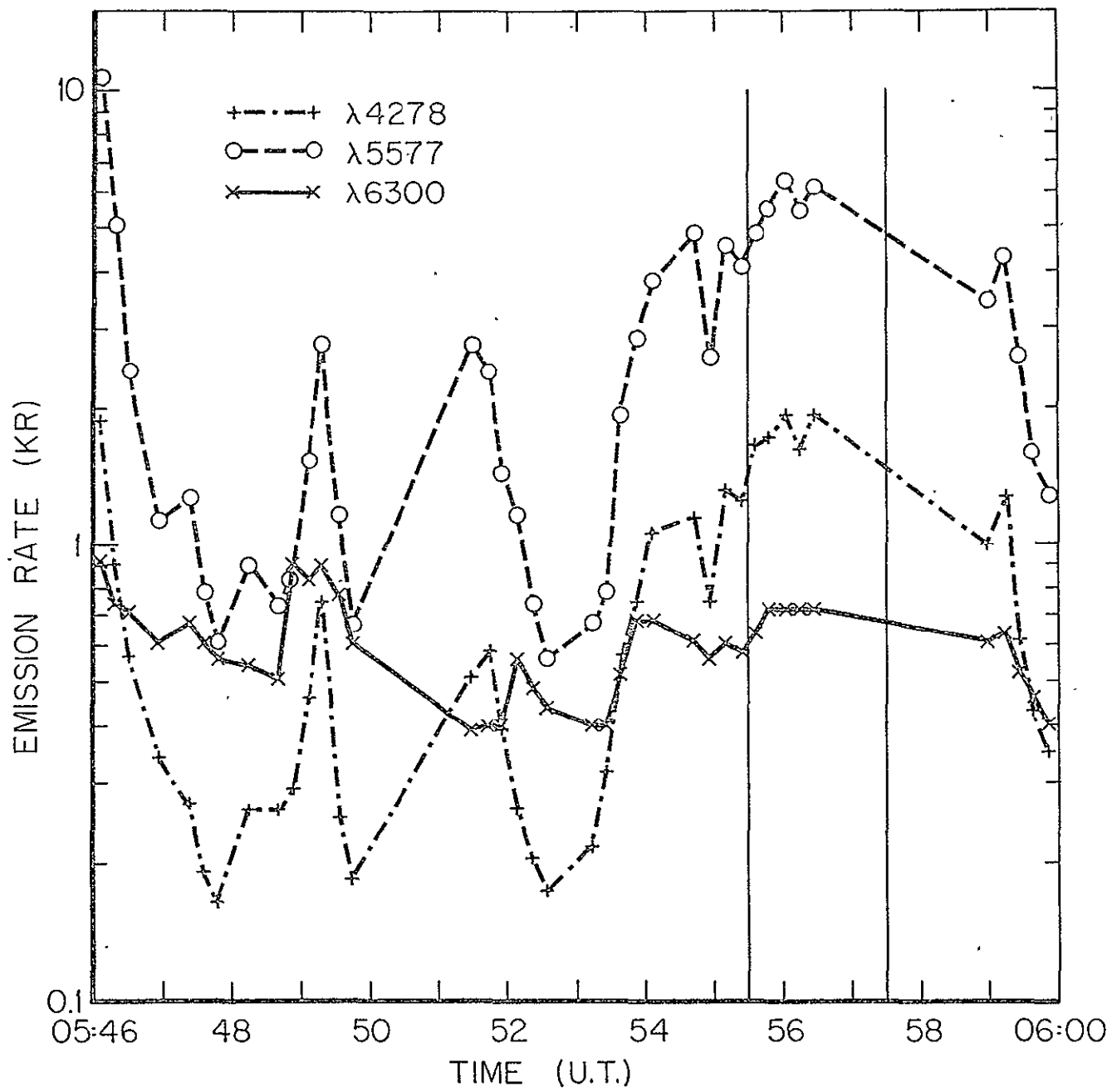


Figure 12

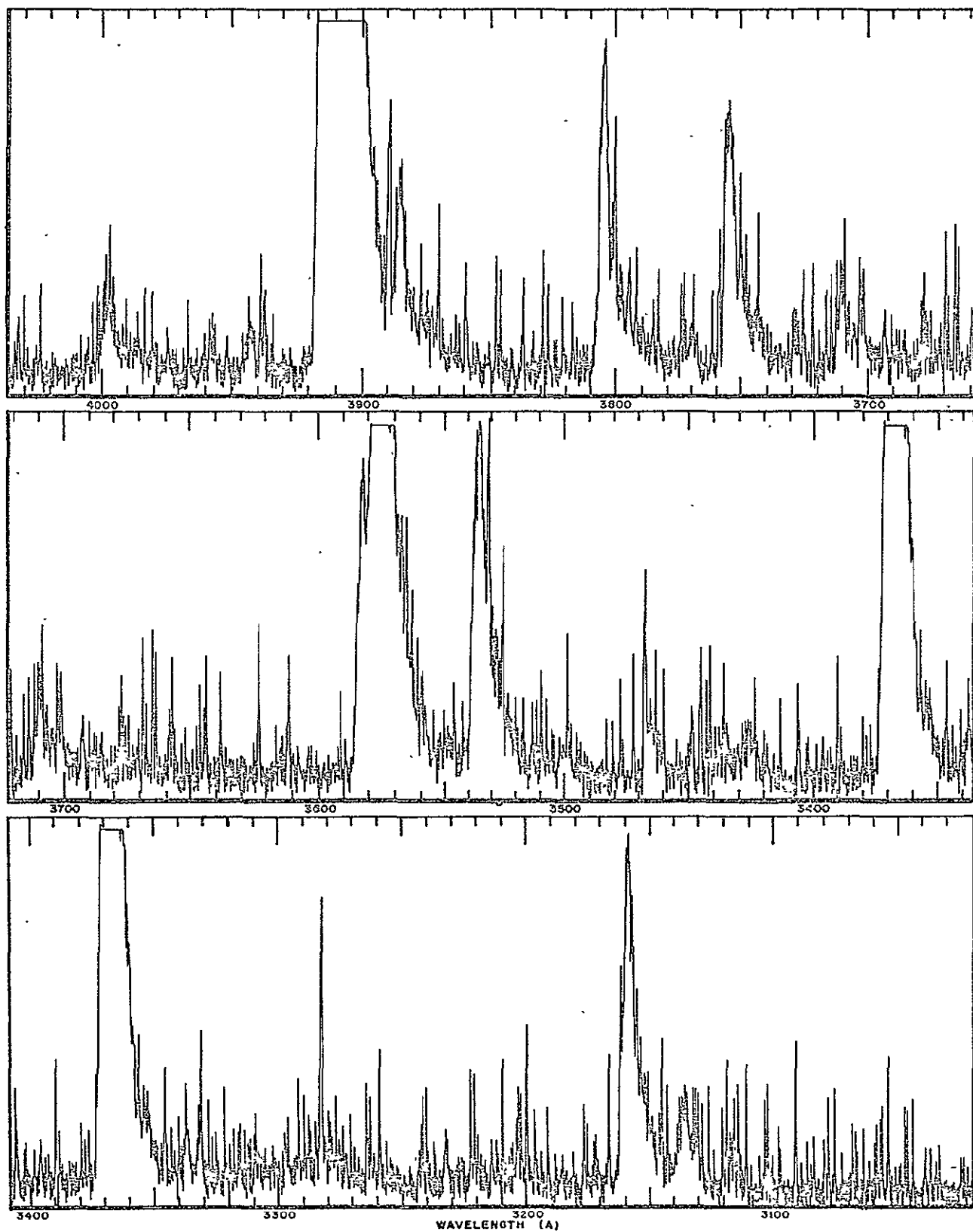


Figure 13

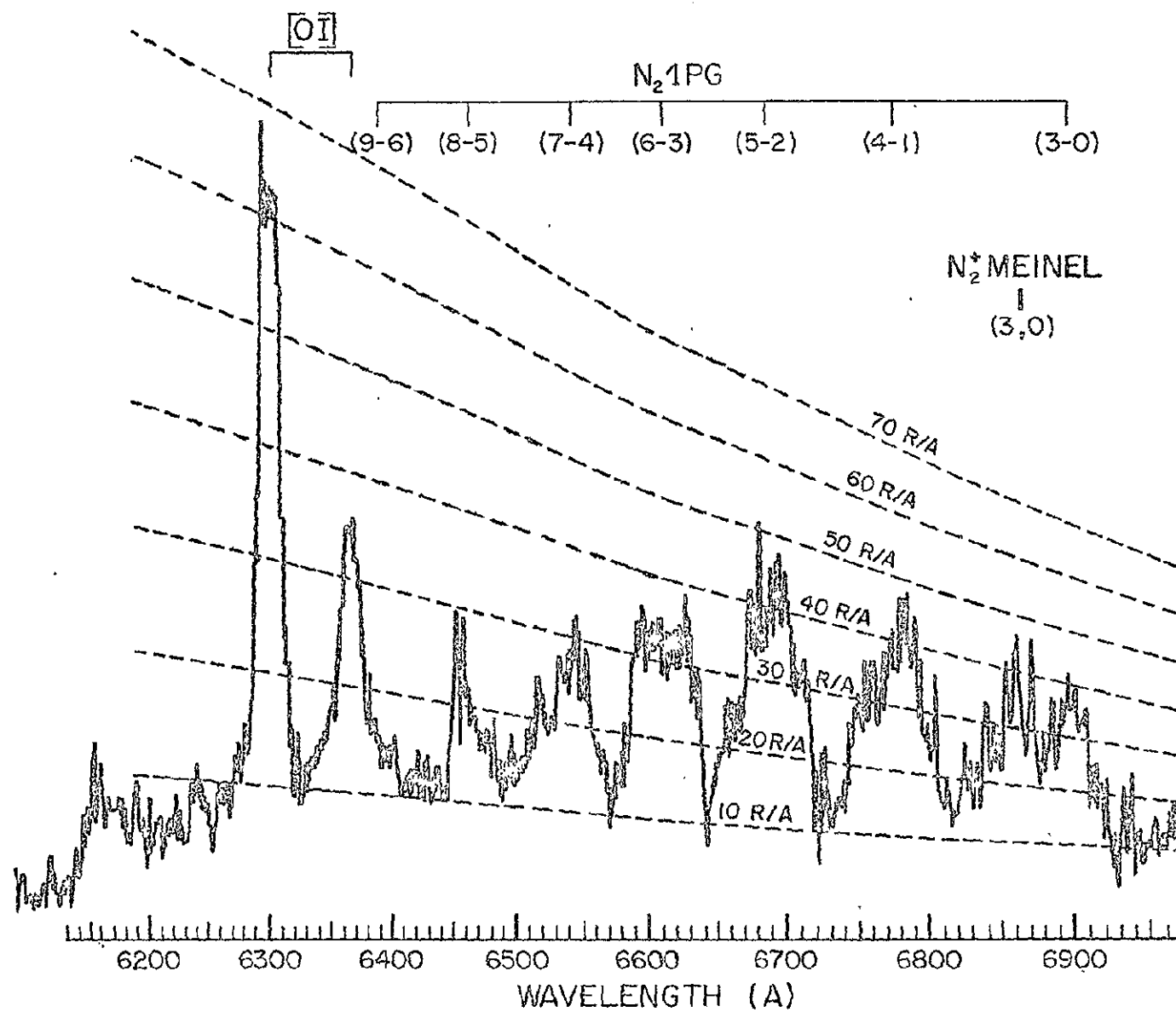


Figure 14

at high gain on the strip chart; this shows the weak features and the noise, while the bright features are clipped. Large amplitude noise spikes can be identified by their width which is less than the profile of a real emission feature. Many auroral emission features can be identified. There are several bands of the $\Delta v = -1, 0, 1, 2, 3$ sequences of the N_2 2PG system; the N_2^+ 1NG (0,0) and (1,1) bands are present, and the (1,0) and (3,2) bands are just resolved from the much brighter (0,1) band of the 2PG system. Observations of the various bands are summarized in Tables 1. through 4. There are four bands of the Vegard-Kaplan system, the (1,9), (1,10) (2,11) and (2,12), that are weak features. The complex structure of the V-K bands causes serious contamination problems from overlapping spectral features. The outstanding atomic emission is the [NI] line at 3466 A. There are other atomic lines present for which we give tentative identifications.

Figure 14 shows a spectral scan in the wavelength region 6200 to 6950 A at 15 A resolution. This region is dominated by the $\Delta v = 3$ sequence of N_2 1PG. The (3,0) band of the system overlaps the (3,0) band of the N_2^+ Meinel system, while the (9,6) band includes the 6364 A line of [OI] and the (0,1) band of O_2^+ 1NG. The prominent atomic feature is the [OI] 6300 A line.

Successive spectra in each wavelength region showed small variations both in the relative intensities of bands within a system and in the absolute intensity of a given band, indicating that small fluctuations in the aurora occurred even during individual 25 sec spectral scans. Fluctuations in aurora are the rule rather than the exception, introducing an observational uncertainty into most spectroscopic measure-

TABLE 1 N_2^+ 1NG

v'	v''	
	0	1
0	3914	4278
	5900 ± 410	1750 ± 200
	5900	1797
1	3582	3884
	408	236

$$\Sigma_{v', v''} = 9230 \pm 500 R$$

wavelength of band head (A)

observed emission rate (R) and relative error

predicted emission rates (Nicholls, 1961;
Shemansky and Broadfoot 1971b)

TABLE 2 N₂ 2PG

v'	v''					
	0	1	2	3	4	5
0	3371	3577	3805			
	2270 ± 290	1114 ± 265	614 ± 55			
	2131	1441	575			
1	3159	3339	3537	3755	3998	
	1208 ± 195	164 ± 26	478 ± 52	460 ± 52	232 ± 30	
	1119	52	508	445	227	
2		3136			3711	3943
		454 ± 82			130 ± 30	115 ± 22
		428			166	131
3			3117			
			169 ± 45			
			121			

$$\sum_{v', v''}^{4,9} = 8700 \pm 1000 R$$

wavelength of bandhead (Å)

observed emission rate (R) and relative error

predicted emission rates (Shemansky and Broadfoot, 1971a, b)

TABLE 3 N₂ 1PG

v'	v''				
	1	2	3	4	5
4	6772 1211 \pm 100				
5		6689 1353 \pm 120			
6			6608 1008 \pm 105		
7				6530 701 \pm 55	
8					6454 522 \pm 45

wavelength (A)

observed emission rate (R) and relative error

TABLE 4 N₂ V-K

v'	v''			
	9	10	11	12
1	3198 425 \pm 110	3425 246 \pm 55		
2			3502 208 \pm 35	3767 185 \pm 30

wavelength (A)

observed emission rate (R) and relative error

ments. The two minute interval selected for analysis showed brightness variations less than 25%. During this period 5 UV and 18 IR spectra were recorded by the spectrophotometers. Two minute averages of corresponding spectra were constructed electronically and from these were obtained the absolute intensities. The averaged spectra are shown in Figures 15 and 16. Signal averaging and some high frequency filtering suppressed much of the noise and provided a spectrum that could be scaled objectively.

Calibration curves (in rayleighs/angstrom) superposed on the spectra include a correction for atmospheric extinction (Elterman and Toolin, 1965), a minor correction at an altitude of 12 km except in the ultraviolet. We have already quoted our estimate of a possible 25% error in the absolute calibration. Additional uncertainty is introduced by noise in the signal and blending of spectral features (discussed in the following paragraph), factors that seriously degrade measurements of weak signals and are the source of relative error in the emission rate. We estimate this uncertainty to vary between $\pm 5\%$, for strong signals, to $\pm 35\%$ for the weaker ones.

A second source of error in determining the absolute intensities of auroral emissions arises from overlap of various features in the spectra. In cases where the features are not completely merged it is possible to separate different bands from a knowledge of their spectral profiles. These profiles can be constructed from the rotational and vibrational distributions of the emitting species and the instrument band pass characteristics. Figure 17 shows, on an expanded wavelength scale, the measured profile of the N_2^+ 1NG (0,0) and (1,1) bands together

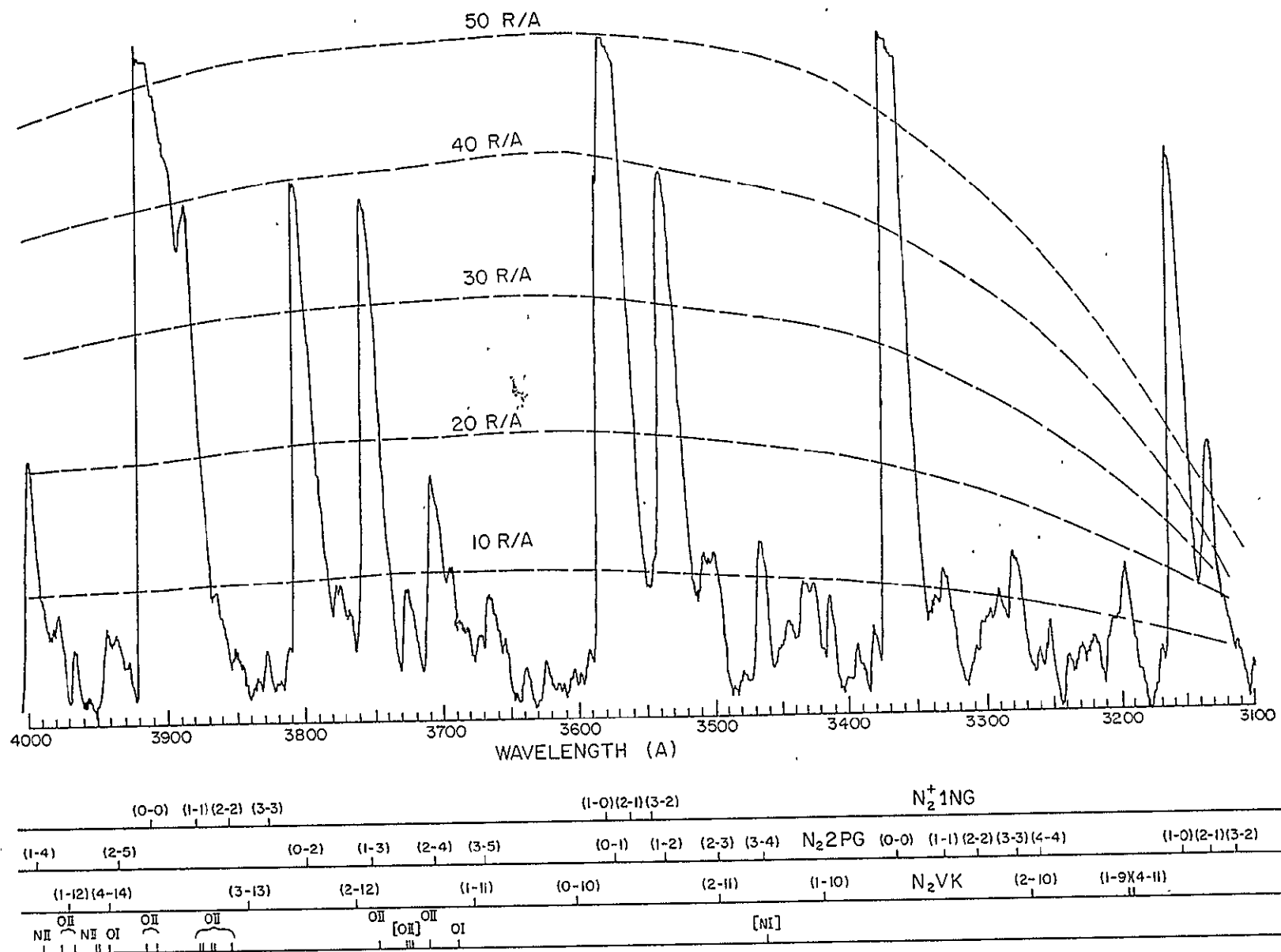


Figure 15

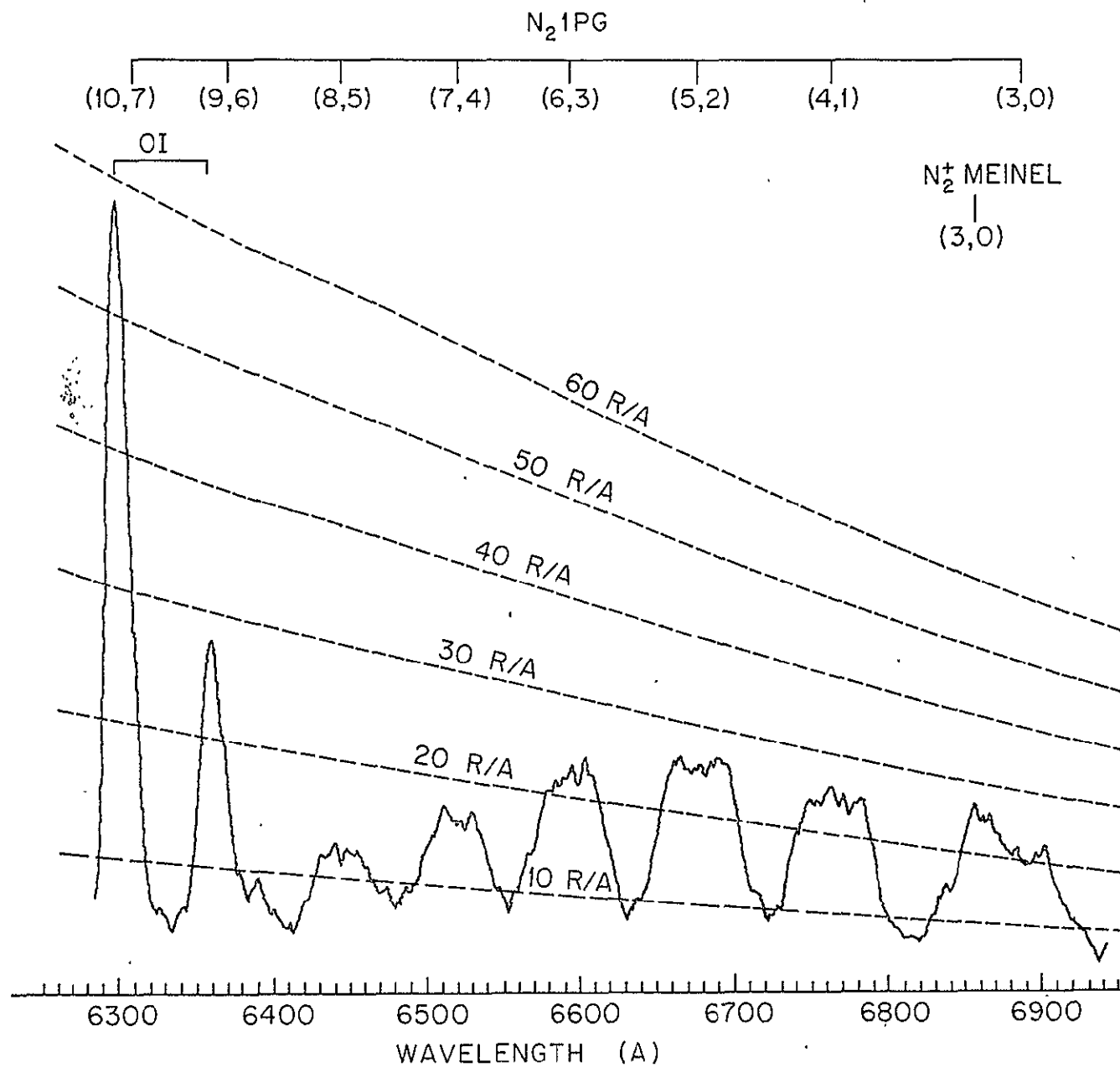


Figure 16

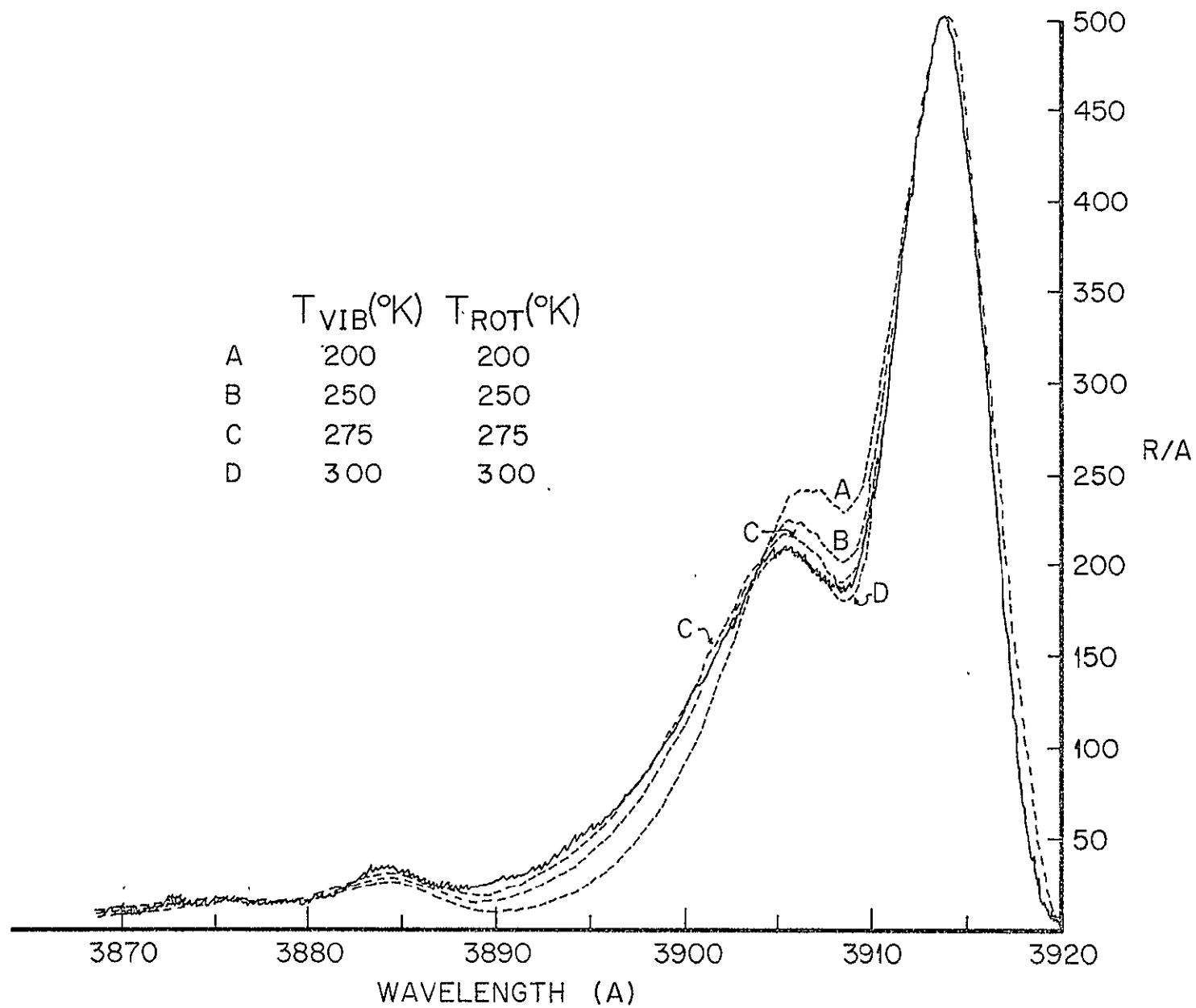


Figure 17

with synthetic profiles of these bands for four assumed vibrational and rotational distributions of N_2 ground state molecules, Boltzman distributions at $T_{vib} = T_{rot} = 200, 250, 275, \text{ and } 300^\circ K$. The synthetic profiles were drawn assuming a triangular shape with a half width of 5A for each rotational line. The best match between observed and theoretical band shapes occurs when the assumed temperature is $275^\circ K$. Having established the instrumental half width and the rotational and vibrational distribution of N_2 , Degen's (1974) synthetic profiles were used to assess, visually, the contribution from each emission in overlapping features. The area under each band and line, in an enlarged version of the spectra shown in Figures 15 and 16, was measured by counting squares on the mm graph paper. The results for molecular bands are presented in the form of Deslandrès tables (Tables 1 through 4). In addition to the observed band intensities and their relative errors, the total emission rates in the N_2^+ 1NG and N_2 2PG systems were computed and emission rates for bands in the wavelength region of interest were inferred, using applicable transition probabilities, in order to assess contributions of overlapping spectral features. It is generally accepted that electron impact from the ground state contributes the bulk of the excitation of the 1NG and 2PG systems permitting the use of appropriate Frank-Condon factors to infer relative populations of the vibrational levels. Observed emission rates listed in the Tables have been corrected for possible contaminating blends. Predicted emission rates for N_2 1PG and N_2 V-K bands are not given in the Tables as part of the observational results because more than one mechanism is responsible for populating various v' levels and the contribution of each is the subject of this report.

Atomic emissions present in the spectra are listed in Table 5. While there are unknown features that appear in the spectra for which identification could be attempted, the low resolution and high noise level lead us to refrain from speculation.

Only 8R of H_{β} radiation were recorded by the tilting filter photometer indicating that proton precipitation during the event contributed a small fraction of the excitation of various auroral emission features (c.f. Eather, 1967).

D. ANALYSIS

The auroral event is modeled by deducing the primary incident electron flux from the optical measurements, computing secondary electron fluxes as a function of altitude, and calculating the electron impact excitation rates of various triplet states in N_2 . Furthermore, the contribution of cascading from the C to B state and B to A state in populating certain vibrational levels is derived.

Using the procedure given by Rees and Luckey (1974) the ratios of emission rates $OI(6300)/N_2^+(4278)$, $OI(5577)/N_2^+(4278)$, and $OI(6300)/OI(5577)$ as a function of $N_2^+(4278)$ emission rate were used to infer a peak energy, α , for the primary electron flux (assuming a maxwellian energy distribution). The value obtained, $\alpha = 2.8 \pm 0.4$, predicts maximum energy deposition at about 115 km. From the wavelength profile of $N_2^+ 1NG(0,0)$ a rotational temperature of 275° K was inferred for the altitude of this spectral feature. According to the U.S. Standard Atmosphere Supplement, 1966, the air temperature at 60°N latitude during winter is 275°K at an altitude of 114 km, consistent with the spectroscopic evidence that the electron flux can be characterized by an energy of a few keV. Because

TABLE 5

Atomic features

Identification	Wavelength (A)	Emission rate (R)
[NI]	3466	69 ± 25
OII (3)	3727	29 ± 15
OII (6)	3954	10 ± 15
NII (6)	3956	
[OI]	6300	724 ± 190
[OI]	6364	220 ± 75

of available computations a value of $\alpha = 3.2$ has been adopted for the model. With an observed 4278 Å emission rate of 1.75 kR we infer from Rees and Luckey (1974) that an electron flux

$$N(E) dE = 8.54 \times 10^7 E \exp(-E/3.2) dE \text{ cm}^{-2}\text{sec}^{-1}\text{keV}^{-1}$$

could have produced the auroral event. The associated energy deposition rate was $9.0 \text{ ergs cm}^{-2}\text{sec}^{-1}$, and the total particle (isotropic) flux was $8.75 \times 10^8 \text{ electrons cm}^{-2}\text{sec}^{-1}$.

The flow chart of the model computations and a description of the procedure are given in previous papers (Rees, 1975, and references therein). Electron impact excitation is given by

$$n(N_2^*) = \int_z n(N_2) \int_{\text{threshold}}^{\infty} \phi(E,z) \sigma(E) dE dz \text{ cm}^{-2}\text{sec}^{-1}$$

where $\phi(E,z)$ is the energy and altitude dependent electron flux, $\sigma(E)$ is the excitation cross section, and $n(N_2)$ is the molecular nitrogen number density. The electron flux derived from the primary spectrum adopted in our model is displayed in Figure 18 for the range of altitudes and energy of interest. [Several measurements of auroral secondary electrons obtained from rocket borne instruments have now been reported in the literature (Sivjee and McEwen, 1976; Feldman and Doering, 1975; Sharp and Hays, 1974; Feldman et al., 1971). Feldman and Doering's (1975): observed spectra can be described by two power law curves, $E^{-3.2}$ between 6 and 20 eV and $E^{-0.9}$ between 20 and 80 eV. Sharp and Hays's (1974) measurements yield a spectrum that is even harder, and that shows an increase in the electron flux above 50 eV. Sivjee and McEwen's

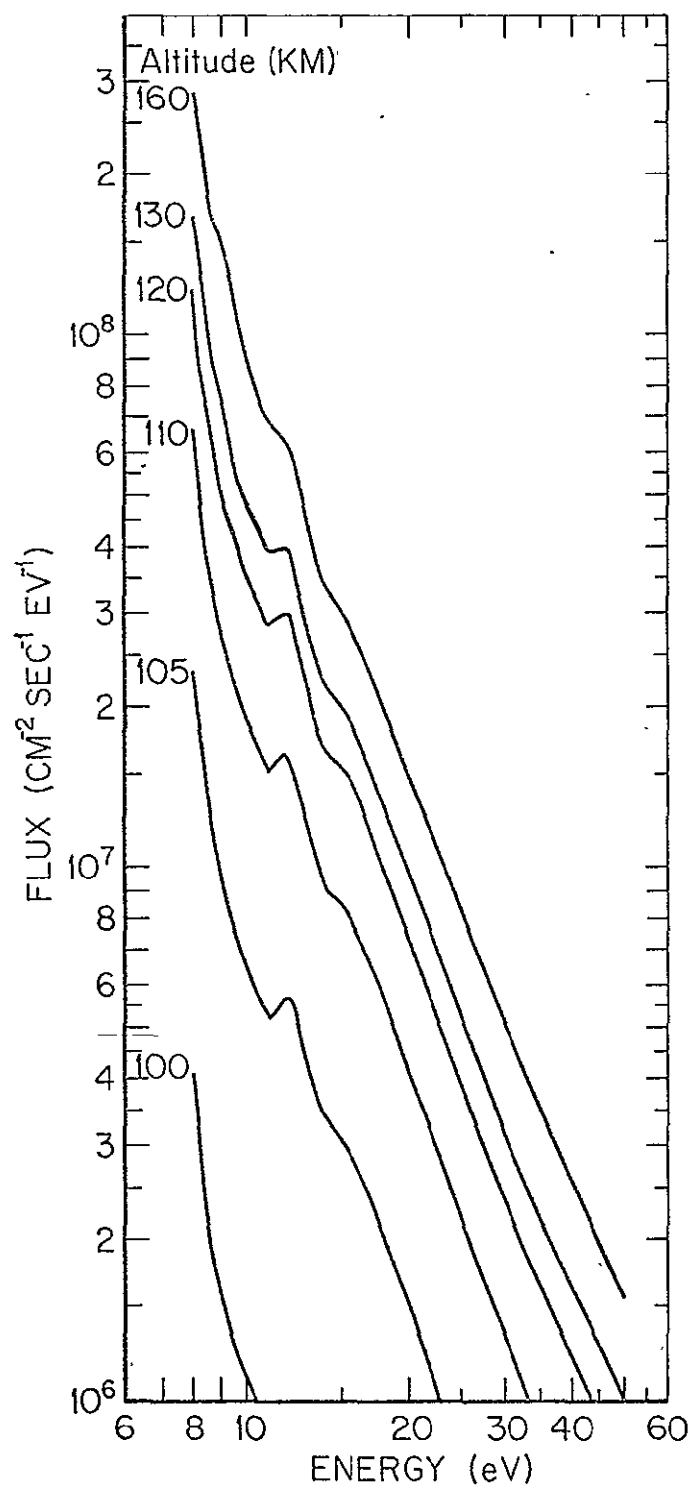


Figure 18

(1975) measurements, however, give spectra that can be described by $E^{-2.7}$ to $E^{-3.1}$ between 20 and 30 eV, and $E^{-1.9}$ to $E^{-2.3}$ between 30 and 50 eV.]

The production rate of secondary electrons has been measured in the laboratory by Opal et al. (1971) and by Borst and Imami (1973), the two measurements showing essential agreement. The stopping power of N_2 , O_2 , and O above 20 eV is dominated by the continuous ionization cross section, quantities that are presumed to be reasonably well known. The above parameters are used in our model to compute the electron fluxes. Our results are in reasonably good agreement with the spectral shape obtained by Borst and Imami (1973) in their laboratory experiment. The auroral spectrum, of course, is a mixture of degraded primary and secondary electrons, however, the magnitude of the primary flux is always considerably smaller than the secondary flux. For example, in our model the average primary electron energy is $2\alpha = 6.4$ keV; each primary electron with this energy produces 183 secondary electrons. Thus, even if the low energy degraded primaries could somehow reach the low altitude region, inaccessible by energy considerations, the contribution would be too small to affect the total flux of secondaries, tertiaries, etc. It has been suggested (e.g. Papadopoulos and Coffey, 1974) that high energy electrons can transfer some of their energy to low energy electrons via wave - particle interaction, an effect that would operate in addition to collisional interactions. This could account for the discrepancy described above; unfortunately, we are not able to take account of the effect in our model computations. Fortunately, this problem does not have a major impact on the excitation rate of the

triplet states of nitrogen because the peak of the cross sections lies between 10 and 15 eV. Indeed, the largest uncertainty in computing the excitation rates derives from the cross sections. This is illustrated in Figures 19, 20 and 23; curves derived from several theoretical computations and from experimental work are displayed for the $C^3\Pi$, $B^3\Pi$, and $A^3\Sigma$ states, respectively. The neutral model atmosphere adopted in all computations is listed in Table 6.

1. The N_2 2PG System

There appears to be good agreement in the peak values of the $N_2 C^3\Pi$ cross section shown in Figure 19, but there are substantial differences in the shapes of the curves. Our model computation uses the cross section given by Cartwright (private communication, 1973, 1975). Since there is no collisional deactivation the emission rate is given by the excitation rate; we obtain 7.9 kR for the band system, which compares well with the value of 8.7 ± 1.0 kR extrapolated from the observed bands.

2. The N_2 1PG System

Two laboratory results and two theoretical curves for the excitation cross section of the total $B^3\Pi$ state are shown in Figure 20; shapes of the curves and peak values differ widely. We have computed the excitation rates only for the observed bands of the 1PG system, and have adopted Shemansky and Broadfoot's (1971a) rates for the $v' = 4$ to 8 levels. The cross sections are displayed in Figure 21; they include contributions from cascading. Emission rates in the observed bands are computed with the transition probabilities given by Shemansky and Broadfoot (1971b); the fraction $A_{v',v''}/\Sigma_v A_{v',v''}$ is listed in Table 7 together with the predicted emission rates.

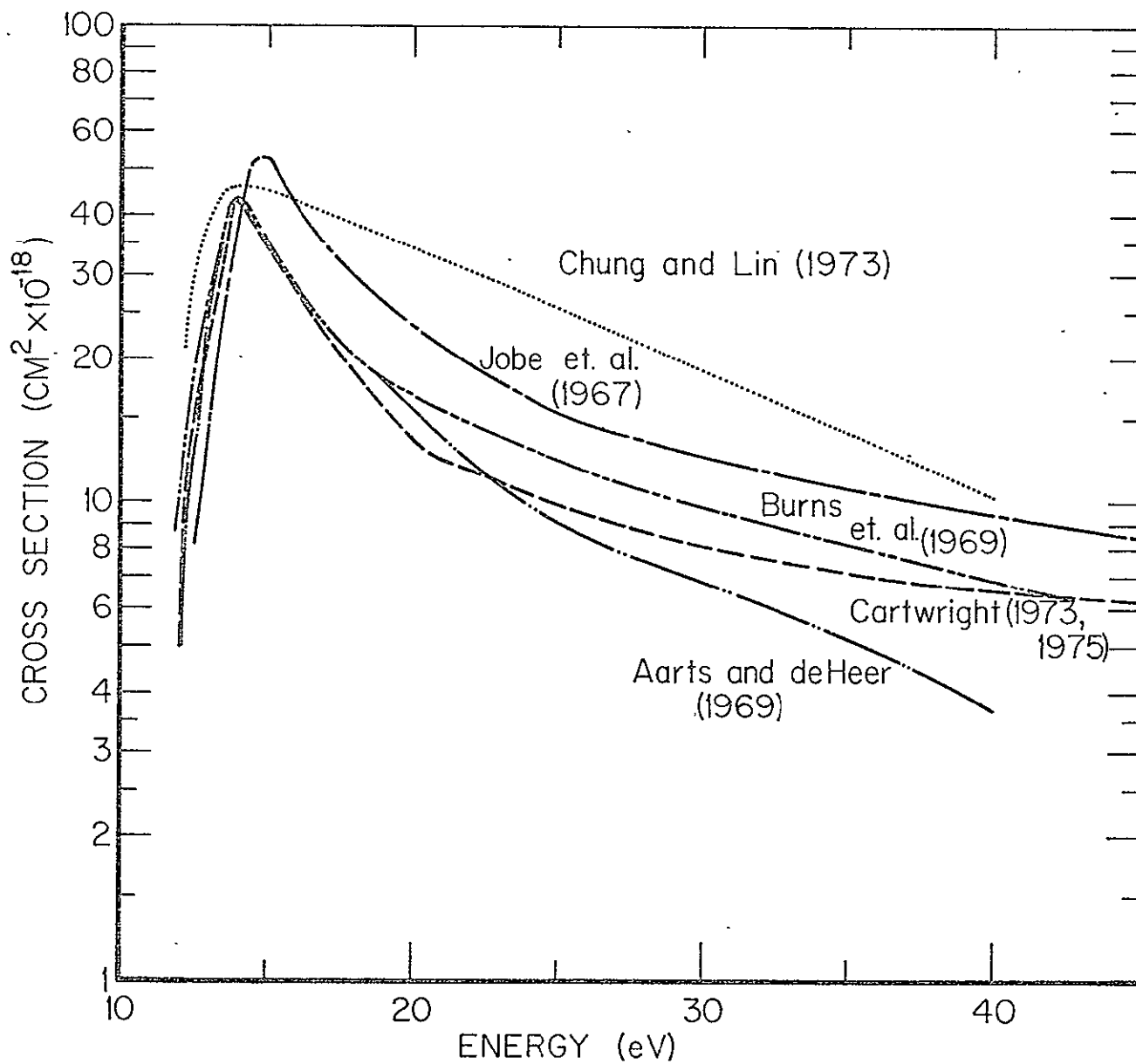


Figure 19

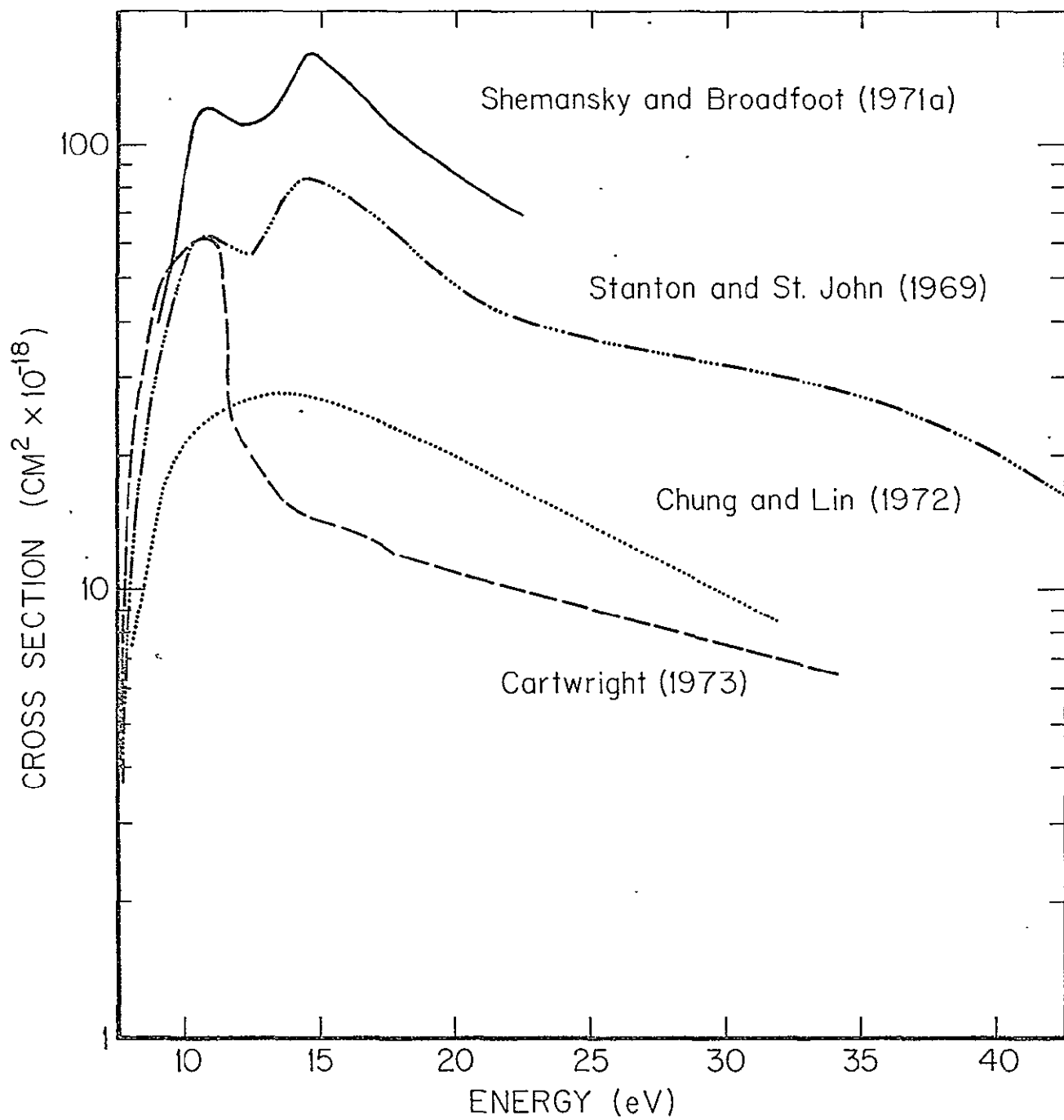


Figure 20

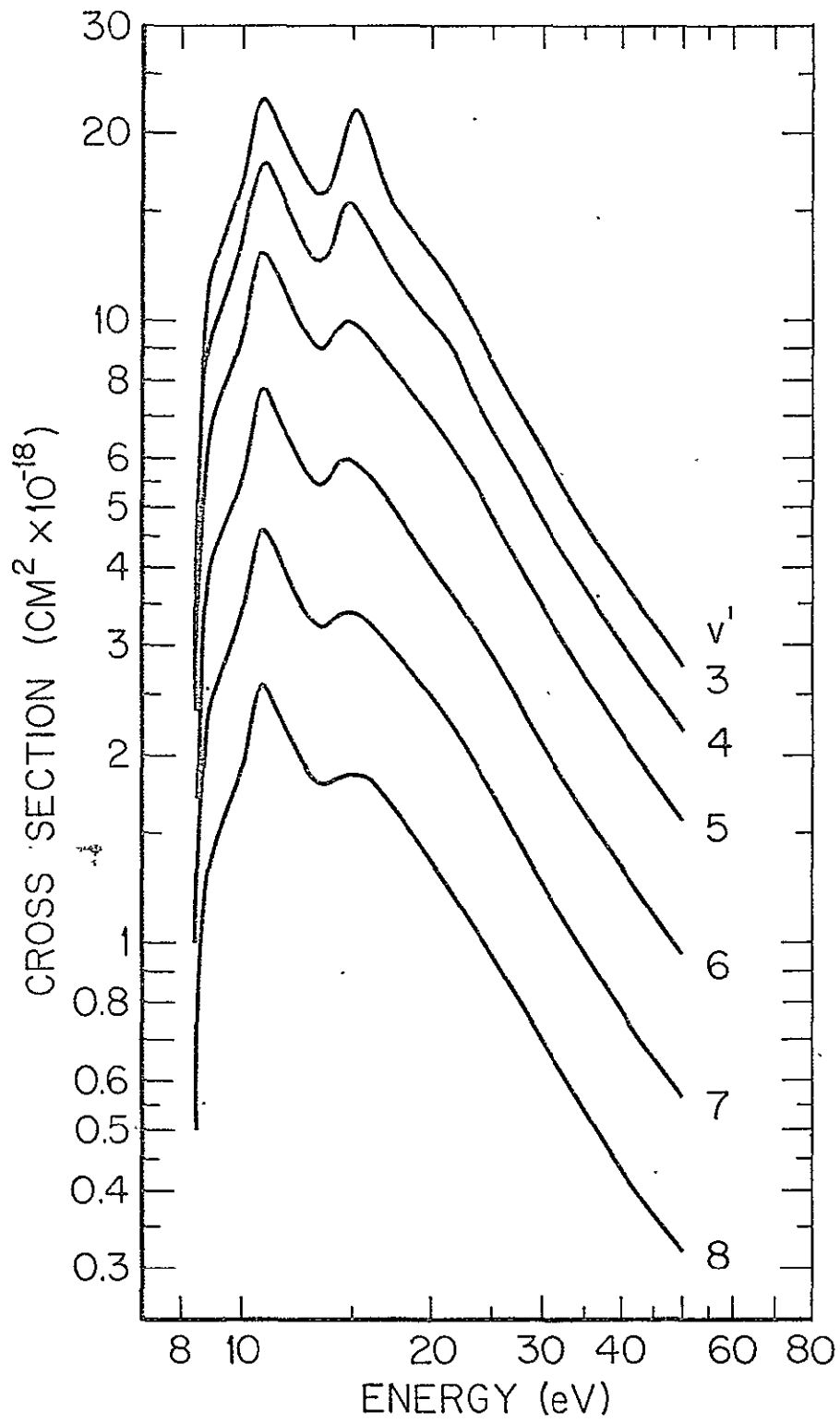


Figure 21

TABLE 6

NEUTRAL MODEL ATMOSPHERE, $T_{\infty} = 1021^{\circ}\text{K}$

ALT (km)	$n(\text{N}_2)$ (cm^{-3})	$n(\text{O}_2)$ (cm^{-3})	$n(\text{O})$ (cm^{-3})	$n(\text{He})$ (cm^{-3})
95	$2.594\text{E}+13^*$	$6.100\text{E}+12$	$1.678\text{E}+12$	$2.041\text{E}+08$
100	$1.040\text{E}+13$	$2.154\text{E}+12$	$1.272\text{E}+12$	$8.184\text{E}+07$
105	$4.309\text{E}+12$	$7.981\text{E}+11$	$7.384\text{E}+11$	$6.900\text{E}+07$
110	$1.808\text{E}+12$	$3.130\text{E}+11$	$4.328\text{E}+11$	$5.750\text{E}+07$
115	$8.720\text{E}+11$	$1.340\text{E}+11$	$2.619\text{E}+11$	$4.787\text{E}+07$
120	$4.430\text{E}+11$	$6.330\text{E}+10$	$1.660\text{E}+11$	$4.024\text{E}+07$
130	$1.409\text{E}+11$	$1.869\text{E}+10$	$7.815\text{E}+10$	$3.000\text{E}+07$
140	$6.330\text{E}+10$	$7.356\text{E}+09$	$4.418\text{E}+10$	$2.411\text{E}+07$
160	$1.835\text{E}+10$	$1.852\text{E}+09$	$1.961\text{E}+10$	$1.800\text{E}+07$
180	$1.131\text{E}+09$	$6.402\text{E}+08$	$1.084\text{E}+10$	$1.486\text{E}+07$
200	$3.179\text{E}+09$	$2.569\text{E}+08$	$6.632\text{E}+09$	$1.284\text{E}+07$
240	$7.707\text{E}+08$	$5.141\text{E}+07$	$2.869\text{E}+09$	$1.021\text{E}+07$
280	$2.135\text{E}+08$	$1.190\text{E}+07$	$1.365\text{E}+09$	$8.455\text{E}+06$
360	$1.943\text{E}+07$	$7.698\text{E}+05$	$3.477\text{E}+08$	$6.078\text{E}+06$

* $2.594\text{E}+13 = 2.594 \times 10^{13}$

TABLE 7 N₂ 1PG

v'	$n(N_2^*)$ (cm ⁻² sec ⁻¹)	v', v''	$A_{v', v''} / \sum_{v''} A_{v', v''}$	Emission rate (R)		C ³ Π to B ³ Π cascade (R)
				predicted	observed	
4	6.0 x 10 ⁹	4,1	0.184	1100	1211±100	89
5	4.3 x 10 ⁹	5,2	0.304	1300	1353±120	99
6	2.6 x 10 ⁹	6,3	0.392	1020	1008±105	64
7	1.5 x 10 ⁹	7,4	0.431	660	701±55	52
8	8.4 x 10 ⁸	8,5	0.418	350	522±45	38

We have evaluated the excitation rate of various $B(v')$ levels by cascading from the C state separately, making use of the observed results on the C state emission rates listed in Table 2 and the relative intensity values given in Table 3.5.2 of Vallance Jones (1971). A graphical extrapolation was made to account for the contribution by $v' > 4$ levels to the population of various v'' levels. The emission rate predicted from the C to B cascade process is listed in Table 7, together with the observed emission rate in each band. The predicted and the observed emission rates are plotted as a function of the v' level in Figure 22. The cross sections of Shemansky and Broadfoot (1971a) yield good agreement between model computations and observations, except for the (8,5) band for which the predicted emission rate is lower than the error bar we have attributed to our observations. Cascading from the C state accounts for less than 10% of the observed band emission rates. Had we adopted the lower experimental cross sections (Stanton and St. John, 1969; McConkey and Simpson, 1969), or the theoretical values (Cartwright, 1973; Chung and Lin, 1972) the predicted emission rates would have been substantially lower than the observed values.

3. The N_2 V-K System

The population rates of the $v' = 1$ and 2 levels of the $N_2 A^3\Sigma$ state by cascade from the $B^3\Pi$ level were computed using the observed emission rates of the (4,1) and (5,2) bands of the B state together with the table of relative LPG band intensities given by Vallance Jones (1971) normalized to correspond to our observed emission rates. The results are given in Table 8. The contribution of electron impact to excitation of the $v' = 1$ and 2 levels was computed from the Frank-Condon

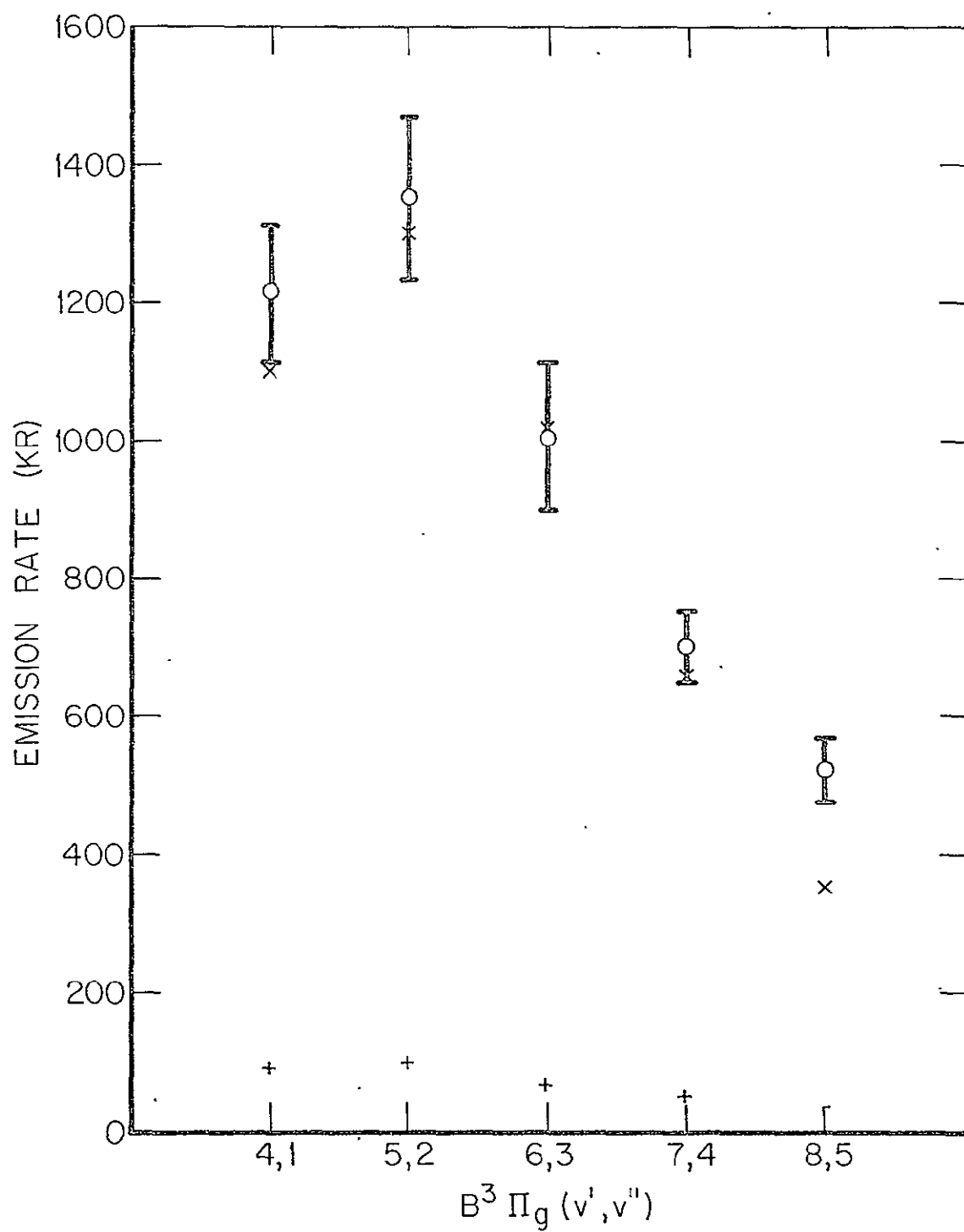


Figure 22

TABLE 8

1PG band v', v''	Observed emission rate (R)	$I(v'v'')/\sum I(v'v'')$ v'	$n(A^3\Sigma(v'))$ ($\text{cm}^{-2}\text{sec}^{-1}$)
4,1	1211	0.115	$v' = 1; 1.05 \times 10^{10}$
5,2	1353	0.165	$v' = 2; 8.2 \times 10^9$

$A^3\Sigma(v')$	$q(0, v')/\sum q(0, v')$ v'	$n(A^3\Sigma(v'))(\text{cm}^{-2}\text{sec}^{-1})$ Cartwright (1975) Borst (1972)		Total $n(A^3\Sigma(v'))(\text{cm}^{-2}\text{sec}^{-1})$ Cartwright (1975) Borst (1972)	
1	0.053	6.3×10^8	2.4×10^9	1.11×10^{10}	1.29×10^{10}
2	0.151	1.8×10^9	6.9×10^9	1.0×10^{10}	1.51×10^{10}

TABLE 8 (Cont'd)

V-K band v', v''	$A_{V'V''}/\sum A_{V''V'V''}$	$\eta (v', v'') (R)$		Observed $A_{110} (v', v'')$ (R)
		Cartwright (1975)	Borst (1972)	
1,9	0.218	2420	2810	425 \pm 155
1,10	0.202	2240	2610	246 \pm 80
2,11	0.200	2000	3020	208 \pm 50
2,12	0.212	2120	3200	185 \pm 50

$A^3_{\Sigma(v')}$	Deactivation rate coefficient, $k (cm^3 sec^{-1})$	
	Cartwright (1975)	Borst (1972)
1	$1.1 \pm 0.5 \times 10^{-10}$	$1.7 \pm 0.5 \times 10^{-10}$
2	$1.5 \pm 0.8 \times 10^{-10}$	$2.4 \pm 0.8 \times 10^{-10}$

factors listed by Borst and Chang (1973) and two of the three cross sections shown in Figure 23. Electron impact excitation rates derived using the Borst (1972) cross sections are about a factor of four larger than the results obtained using the Cartwright (1975) cross sections, and a factor of eight would derive from the Chung and Lin (1972) cross section. Cascading from the B state still provides the largest contribution to the excitation rate of $v' = 1$ but for $v' = 2$ the two sources become comparable using the larger of the two cross sections. The transition probabilities given by Shemansky (1969) were then used to predict the emission rates in the observed bands, in the absence of collisional deactivation. Details are given in Table 8. The predicted emission rate is substantially larger than the observed values implying strong quenching in the aurora under investigation. Assuming that only the cascade and electron impact processes described above contribute to the excitation a quenching rate may be deduced and a rate coefficient, k , derived for a given quenching specie. Quenching by atomic oxygen dominates at all altitudes, therefore,

$$4\pi\Omega (N_2 (V-K)) = \int_z \frac{n(N_2^*)}{A_{v'v''} + k n(O)} dz$$

The altitude profile of the energy deposition rate has been adopted for computing the band excitation rate. The derived rate coefficients are given in Table 8. The uncertainty in the quenching coefficient for $v' = 1$ results principally from the uncertainty in deriving the absolute emission rates of the bands from the spectra. In the case of the $v' = 2$ level an even larger systematic uncertainty lies in the electron impact

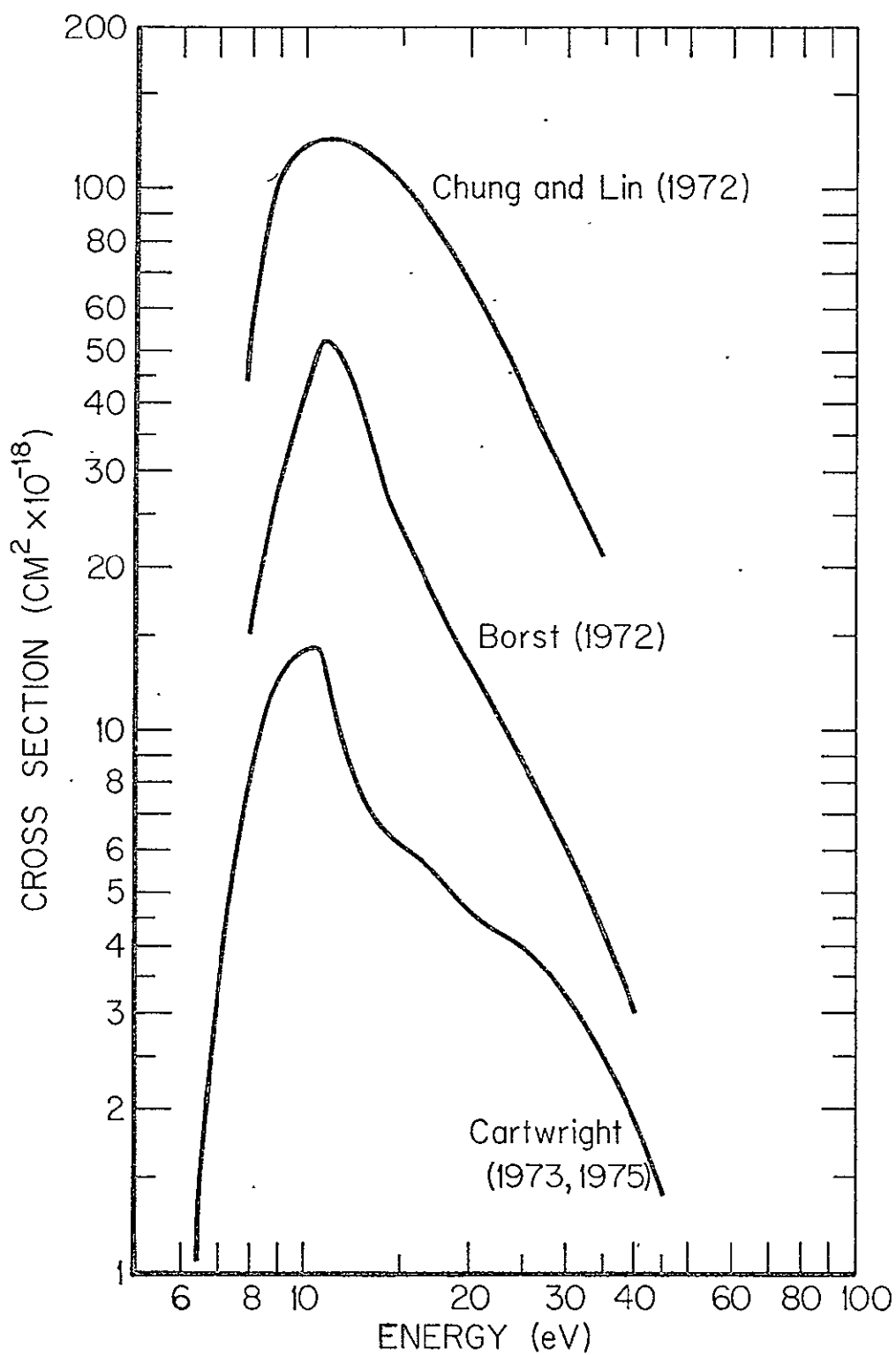
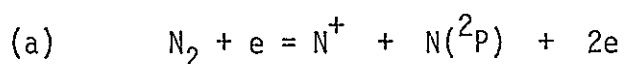


Figure 23

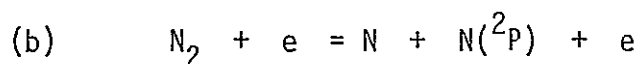
excitation cross section. Although we have invoked only one quenching species, we do not rule out the possibility that there may be more than a single deactivation mechanism. Quenching of the N_2 Vegard Kaplan Bands has been discussed by Vallance Jones and Gattinger (1975), Gerard (1975), Shemansky et al., (1971) and Sharp (1971).

4. [NI] 3466

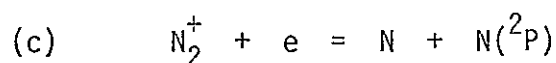
The emission feature at 3466 Å is identified with the $^4S - ^2P$ transition in the $2p^3$ ground configuration of NI. There are several possible sources for the excited state and the principal ones probably are dissociative ionization of N_2



dissociation of N_2



and recombination of N_2^+



None of the cross sections for the production of $N(^2P)$ by the above three reactions have, as yet, been measured. Electron impact excitation of N to the 2P state is probably small by comparison with the above processes in the low altitude aurora under investigation. The radiative lifetime of the 2P state is 12 sec and collisional deactivation by O_2 , NO, and O_2^+ is important. The respective rate coefficients that have been used are 5×10^{-12} , 2.2×10^{-11} , and $1.8 \times 10^{-10} \text{ cm}^3 \text{ sec}^{-1}$. Assuming

that the fraction of N atoms produced in the 2P level by reaction (c) is 0.05 our model computation requires the corresponding fraction for reactions (a) and (b) to be 0.03 in order to derive the observed emission rate of 69 R. An altitude profile of the emission feature would be desirable to further elucidate the problem.

5. Other atomic features

Table 5 lists additional atomic features that are identified with reasonable confidence. The feature at 3727 Å is associated with an allowed transition in OII (multiplet 3) rather than the forbidden transition in [OII] at the same wavelength. The latter would be completely quenched in the low altitude aurora under investigation; a production rate appropriate to this aurora yields a predicted [OII] λ 3727 emission rate of less than one rayleigh. Another line of the allowed multiplet just barely appears in the spectrum at 3749 Å, riding on the wing of the N_2 2PG (1,3) band. A third line of the multiplet at 3713 Å is too faint to be detectable in the spectrum at hand.

The spectral feature at 3955 Å is identified with an OII (6) line and an NII (6) line at 3954 Å and 3956 Å respectively. The appearance of allowed transitions of O^+ and N^+ is associated with the production of highly excited states in dissociative ionization reactions.

E. DISCUSSION AND CONCLUSIONS

An analysis of several bands of the N_2 2PG, N_2 1PG and N_2 V-K systems emitted in a well documented two-minute auroral event suggests the following conclusions regarding the excitation mechanisms of the $C^3\Pi$, $B^3\Pi$ and $A^3\Sigma$ levels.

- (1) Within the uncertainties of the observations the $v' = 0$ to 3 levels of the $C^3\Pi$ electronic state are populated by electron impact, and the cross sections shown in Figure 9 predict absolute emission rates in good agreement with the observations.
- (2) Cross sections for excitation of the $v' = 4$ to 8 levels derived by Shemansky and Broadfoot (1971a) from laboratory measurements of the optical excitation functions predict well the 1PG bands of the $\Delta v = 3$ sequence observed in the auroral event under investigation. An independent analysis, based on observed 2PG bands, predicts a contribution to the 1PG bands by cascading from the C state of less than 10%. Contributions from additional systems ($W^3\Delta$, $A^3\Sigma$) are not required but could already be included in the measured optical excitation functions.
- (3) The $A^3\Sigma$ $v' = 1, 2$ levels are populated principally by cascading from the B state but the contribution from electron impact excitation of N_2 could be appreciable if the large cross sections in Figure 13 are correct. Our measurements cannot resolve this question because collisional deactivation must be invoked in any case, and a higher production rate would only require a larger quenching rate to match the observations. Adopting the deactivation coefficients derived by Vallance Jones and Gattinger (1975), $k(v' = 1) = 9.2 \times 10^{-11} \text{ cm}^3 \text{ sec}^{-1}$ and $k(v' = 2) = 1.2 \times 10^{-10} \text{ cm}^3 \text{ sec}^{-1}$, would favor the lower values of Cartwright (1975) for electron impact excitation. Observations of the N_2 triplet bands in aurora excited

at an altitude where collisional deactivation of $A^3\Sigma$ state becomes small would provide a basis for evaluating the electron impact excitation contribution to this state.

Perhaps the best opportunity to study this problem further will become available with the Space Shuttle. Specifically, an electron accelerator may be used to excite an artificial aurora over a wide range of electron energies in a low pressure, large volume region. Spectroscopic analysis of the luminosity from the ultraviolet into the infrared would extend measurements from the shortest wavelength V-K bands to the longest wavelength 1PG bands.

In addition to the analyses described on the preceding pages, there is enough data available to study the following three auroral problems.

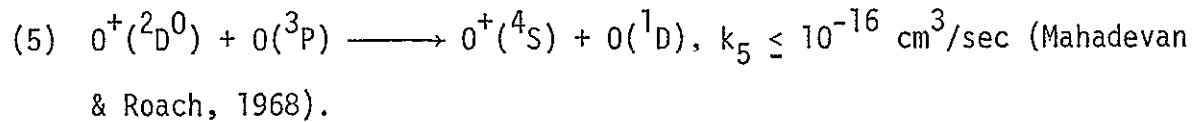
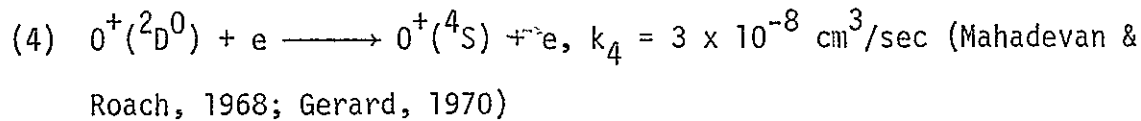
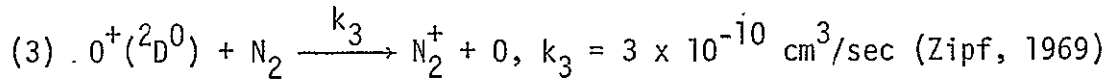
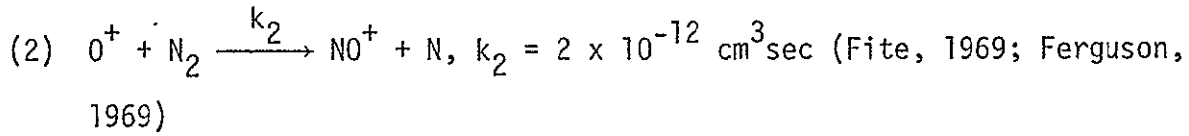
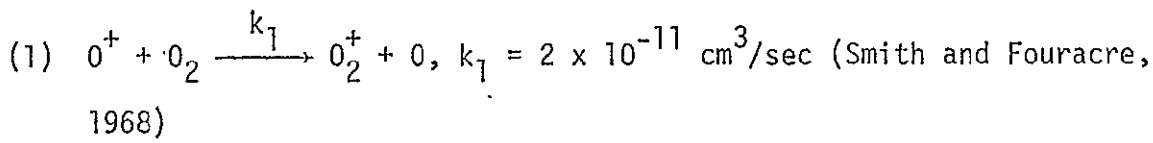
IV. [OII] 3726-3729A EMISSIONS FROM AURORAS

Several observations of [OII] 'nebulium' line emissions from stellar objects have been reported (Bowen, 1928; Menzel and Aller, 1941; Aller and White, 1949; Seaton and Osterbrock, 1957). These measurements triggered extensive theoretical calculations (Garstang, 1952; Seaton, 1953, 1955; Seaton and Osterbrock, 1957) of transition probabilities as well as quenching strengths for various O^+ metastable states in an attempt to relate the observed 3726/3729 ratios to densities and temperatures of electrons in the emitting regions. Recently, interest in these emissions from metastable $^2D^0$ states of O^+ has resurfaced, this time among aeronomers, primarily because of the importance of O^+ in the ion chemistry of the F region. The charge exchange reaction between $O^+(^2D^0)$ and N_2 may be an additional source of N_2^+ ($A^2\pi_u, v'=1$) (Omholt, 1959; Dalgarno and McElroy, 1966; Feldman, 1973) in dayglow, twilights and in auroras; not only would this reaction boost N_2^+ Meinel band emissions from ordinary auroras but also by increasing N_2^+ ions it would enhance N_2^+ Meinel and ING band emissions in dayglow, twilights and sunlit auroras where these emissions are produced by resonant scattering of solar electromagnetic radiations (Broadfoot, 1971; Feldman, 1973). The relative importance of charge transfer reaction between $O^+(^2D)$ and N_2 as a source of N_2^+ ($A^2\pi_u, v'=1$) depends on the magnitude of the rate coefficient of this reaction, a parameter that has not yet been quantitatively determined.

During periods of particle precipitations in the atmosphere, atomic oxygen ions are produced both through ionization of oxygen atoms as well as via dissociative ionization of O_2 . The production rate of O^+ is

related to the total ionization rate (Rees and Jones, 1973), a quantity which is independent of details in the energy spectrum of the precipitating electrons and can be derived either from laboratory data (Rees, 1963) or from theoretical calculations (Banks et al., 1973). According to Seaton (1953), relative numbers of $O^+(^4S)$ to $O^+(^2P)$ produced by electron impact on atomic oxygen are in the ratio of 2:4:4 while laboratory studies of electron impact on O indicate that about $35 \pm 15\%$ of the ions are left in the excited states (Stebbing et al., 1966). Now recent rocket and ground-based measurements of auroral 7319-7330 emissions by Swanson (1974) show that the number of $O^+(^2P)$ produced in an aurora is less than 1% of all the O^+ ions produced. Hence almost all of the metastable O^+ ions observed by Stebbings et al. (1966) must have been in 2D state. Apparently both Seaton's (1953) theoretical calculations and Stebbings et al.'s (1966) laboratory measurements imply about 40% efficiency for populating the $O^+(^2D)$ level during ionization of atomic oxygen through particle impact. While no such information is available for dissociative ionization process, this poses no problem in assessing the production rate of $O^+(^2D)$ since calculation based on atmospheric densities show that dissociative ionization of O_2 contributes less than 10% of the total O^+ production at altitude where quenching of $O^+(^2D)$ is relatively less severe.

Because of the relatively long radiative lifetime of $O^+(^2D)$ (Seaton and Osterbrock, 1957), quenching of this species by ambient atmospheric particles through the following reactions depopulate most of the $O(^2D)$ through nonradiative transitions:



An expression for the intensity of [OII] UV doublet can be derived in terms of the production and loss rates of $O^+(^2D)$. It is possible to evaluate this expression for different values of the quenching rates to derive a set of reaction rates which lead to a computed 3726-3729 intensity value in agreement with the observed intensity. In the following section we detail the procedures employed in computing both the [OII] UV doublet and N_2^+ ING (0,0) band intensities.

The sum of the intensities of 3726 [$O^+(^2D_{3/2} \rightarrow ^4S_{3/2})$] and 3729 [$O^+(^2D_{5/2} \rightarrow ^4S_{3/2})$] emissions is given by the following equation:

$$(6) \quad I(3726-3729) = \frac{0.4 * n(O^+) * A_{\text{mult}} [O^+(^2D^0 \rightarrow ^4S_{3/2})]}{[1/\tau(O^+(^2D^0)) + (k_2+k_3) n(N_2) + k_1 n(O_2) + k_4 n(e) + k_5 n(O)]}$$

where $A_{\text{mult}} = \{\tilde{\omega}(^2D_{3/2})A(^2D_{3/2} \rightarrow ^4S_{3/2}) + \tilde{\omega}(^2D_{5/2})A_{\text{mult}}(^2D_{5/2} \rightarrow ^4S_{3/2})\} / \{\tilde{\omega}(^2D_{3/2}) + \tilde{\omega}(^2D_{5/2})\}$, $\tilde{\omega}$ stand for statistical weight of the upper level, A is the Einstein coefficient for simultaneous emission, τ is the radiative lifetime of $O^+(^2D)$ level $(= 1 / \{A_{\text{mult}}[O^+(^2D \rightarrow ^4S)] + A[O^+(^2D_{3/2} \rightarrow ^2D_{5/2})]\})$ and $n(O^+)$ is the production rate of O^+ ions. For the case of ionization of atomic oxygen through electron impact

$$(7) \quad n(O^+) = 0.56n(O)q/\alpha$$

where $\alpha = 1.15 n(N_2) + 1.5 n(O_2) + 0.56 n(O) + 0.43 n(He) + 0.8 n(H)$ and q = total ionization rate of all atmospheric species.

Contribution to $n(O^+)$ from dissociative ionization is given by

$$(8) \quad n(O^+) = 0.5n(O_2^+)$$

where

$$(9) \quad n(O_2^+) = n(O_2)q/\alpha$$

The intensity of N_2^+ ING (0,0) band emission can be computed from the relation

$$(10) \quad I(3914) = (0.9n(N_2)q/\alpha) / 14$$

Equations (7) through (10) have been taken from the paper by Rees and Jones (1973).

The most recent values of Einstein coefficients for O^+ are those calculated by Seaton and Osterbrock (1957). According to these authors $A[O^+(^2D_{3/2} \rightarrow ^2D_{5/2})] = 1.3 \times 10^{-7}$, $A[O^+(^2D_{3/2} \rightarrow ^4S_{3/2})] = 1.699 \times 10^{-4}$ and $A[O^+(^2D_{5/2} \rightarrow ^4S_{3/2})] = 4.88 \times 10^{-5}$. We have chosen calculated rather

than adjusted values since the latter are based on observations of the 3726-3729 ratios from stellar regions where physical conditions differ significantly from those in the E and F regions of the terrestrial atmosphere. The above values of A yield $A_{\text{mult}}[O^+(^2D^0 \rightarrow ^4S)] = 9.724 \times 10^{-5} \text{ sec}^{-1}$ and $\tau[O^+(^2D^0)] = 1.02679 \times 10^4 \text{ sec}$, both of which are significantly different from those derived by Garstang (1956).

The radiative lifetime of $O^+(^2D)$ is longer than the characteristic time for $O^+(^2D)$ quenching by reactions (1) through (4). Reaction (5) can be ignored since $k_5 n(O_2)$ is less than 10^{-5} at all altitudes above 100 kms. Of the five quenching mechanisms listed above, (3) appears to be the most important one below 300 kms while (4) may be as effective as (3) above this height. These remarks apply only to auroras excited by electrons penetrating down to around 110 kms.

The quenching reactions (1) through (5) can be divided into two groups. Those involving all O^+ ions can be studied in the laboratories and their reaction rates have been accurately determined. Reactions (1) and (2) fall in this category; the rate coefficient for (1) has been measured by Smith and Fouracre (1968) as well as by Ferguson et al. (1969) while the rate for reaction (2) has been determined by several investigators (see Fite, 1969 and Ferguson, 1969, for references). The remaining three quenching mechanisms all involve O^+ ion in a specific metastable state. Since it is difficult to isolate and control a beam of $O^+(^2D^0)$ ions for laboratory studies no direct quantitative determination of the rate coefficients for reactions (3) to (5) have been reported so far. We can discount reaction (5) because of its small effective cross-section (Mahadevan and Roach, 1968). Various investi-

gators (e.g., Gerard, 1970; Broadfoot, 1971) have referenced Zipf (1969) as a source for the rate coefficient of reaction (3). While no specific reaction is mentioned by Zipf (1969) he does list a rate of 3×10^{-10} cm³/sec for O⁺ quenching by N₂. Since the author quotes 1×10^{-12} for reaction (2) the higher rate quoted must refer to reaction (3) though this is not clearly spelled out. Zipf (1969) references Dalgarno and McElroy (1966) and Stebbings et al. (1966) for k₃ value of between 1 and 0.3×10^{-9} cm³/sec. A value of 2×10^{-9} cm³/sec for k₃ was selected by Dalgarno and McElroy (1966), together with modified rate coefficients for N₂⁺ interacting with O, O₂ and e, to explain certain dayglow data. In an experiment based on attenuation of an ion beam during passage from an ion source to a collector through a chamber containing target gas (e.g., N₂), Stebbings et al. (1968) measured k₃ values of between 1 and 3.6×10^{-9} cm³/sec. Stebbings et al.'s identification of O⁺(²D⁰) as the ion responsible in reaction (3) was based on their observation of zero cross-section for this reaction at and below the threshold energy for excitation of O⁺(²D) from O(³P) by electron bombardment. On the otherhand, Banks and Holzer (1969) list a theoretically derived rate coefficient of 6.9×10^{-10} cm³/sec from (3). All these values for k₃ are higher than the rate coefficient of 3×10^{-10} cm³/sec listed by Zipf (1969). Ferguson (1969) and Feldman (1973) quote Turner et al. (1969) as a source reference for k₃ = 1×10^{-10} cm³/sec while the data presented by Turner et al. (1963) are identical to those presented by Stebbings (1966). Hence, k₃ values derived both from laboratory measurements and dayglow studies are higher, by about an order of magnitude, than the value quoted by Zipf (1969).

The other important quenching mechanism is reaction (4). Mehadevan and Roach (1968) as well as Gerard (1970) quote Seaton and Osterbrock (1957) as a source for $k_4 = 3 \times 10^{-8} \text{ cm}^3/\text{sec}$. Since this particular figure does not appear anywhere in the latter, it must have been computed using collision strength Ω calculations of Seaton and Osterbrock (1957). The quenching rate coefficient k_4 is related to Ω and electron temperature T_e through the following equation given by Chamberlain (1961):

$$(11) \quad k_6 = \frac{h^2}{2\pi m^2} \left(\frac{m}{2\pi k T_e} \right)^{1/2} \left[\frac{\Omega(^2D_{3/2} \rightarrow ^4S_{3/2})}{\omega(^2D_{3/2})} + \frac{\Omega(^2D_{5/2} \rightarrow ^4S_{3/2})}{\omega(^2D_{5/2})} \right]$$

Using Seaton and Osterbrock's collisions strength values we get

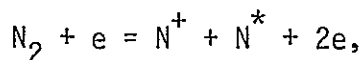
$$k_6 = \frac{2.208 \times 10^{-6}}{\sqrt{T_e}}$$

For values of T_3 found in the E and F region, k_4 is approximately $3 \times 10^{-8} \text{ cm}^3/\text{sec}$. This quenching rate based mostly on theoretical calculations appears to be too high; it makes electron quenching of $O^+(^2D)$ more important than reaction (3) above 300 km even in westward traveling surges where maximum electron densities occur around 110 kms while the F region electron density is only $1 \times 10^4 \text{ cm}^3$. It would completely quench $O^+(^2D)$ during periods of low energy ($< 1 \text{ kev}$) electron precipitations when the bulk of the ionization is produced by the F region and the electron density there may be higher than 10^6 cm^3 .

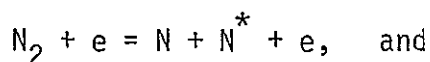
V. EXCITATION OF NI 3466 AND 5200 EMISSIONS

The 3466 and 5200 emissions result from the $4S-2P$ and $4S-2D$ transitions in the $2P^3$ ground configuration of NI. There are several possible sources for the excited states, the principals being

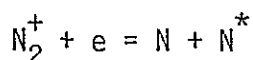
(a) dissociative ionization of N_2



(b) dissociation of N_2



(c) recombination of N_2^+



None of the cross-section for the production of $N(^2D)$ and $N(^2P)$ by the above three reactions have yet been measured. Electron impact excitation of N to 2D and 2P states is probably small in the most frequent occurring relatively low altitude auroras. The radiative lifetime of the 2P state is 12 sec while that for 2D is 26 hours. Hence, collisional deactivation is important.

The fraction of N atoms produced in the 2D and 2P levels in the above three reactions is unknown. This information and the effective quenching of the two levels may become available from the analysis of some of the spectroscopic and photometric measurements of NI 3466 and 5200 emissions made during the 1969 Airborne Auroral Expedition.

VI. OPTICAL EMISSION FROM O_2 , NO AND OTHER SPECIES IN A WESTWARD TRAVELING SURGE

The UV and IR auroral spectra from a westward traveling surge observed on November 26, 1969, aboard NASA's CV 990, contain several unidentified features. Some of these may represent emissions from $NO\beta$ bands, O_2^+ 2nd negative bands and O_2^+ 1NG bands. To date no conclusive evidence for either $NO\beta$ bands or O_2^+ 2nd negative bands in auroras has been reported in the literature. Hence, it is scientifically worthwhile to analyze the unidentified features in the spectra from westward traveling surge to establish whether they do originate from NO and O_2 . The study of O_2^+ 1st negative bands in the IR is important in understanding the dissipation of the auroral particle energy in the excitation of various atmospheric species.

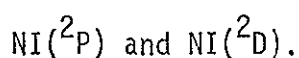
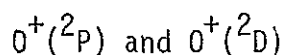
VII. SUMMARY

The preceding presentation of the results from a coordinated analysis of airborne auroral measurements clearly demonstrates the usefulness of combining various sets of data in attacking research problems in auroral physics. The scientific basis for continuing such analyses has been outlined and it is hoped that funds for this work will be made available.

The most obvious and striking feature of the 1968 and 1969 Airborne Auroral Expeditions was the lack of close coordination among various experimenters. Most of the experiments were designed to satisfy the limited scientific goals of the individual experimenters. There was little, if any, attempt to coordinate the various measurements with a view to attacking problems which require a larger set of data and hence involve the analyses of measurements made by different research groups. Even the fields of view of the detectors used by different experimenters, their look directions, mode of operations, data format and recording procedures differed greatly. Recognizing that the scientific objective of individual experimenters will always dominate the planning of the experiment, it is argued here that with a little coordination among the experimenters it is possible to standardize some of the parameters listed above without in any way compromising on the legitimate data requirements of the various researchers. The choice of the experiments, however, should be guided by the scientific need to cover the widest possible segment of the spectrum (3000Å to 5μ) of electromagnetic radiation from the aurora instead of duplicating efforts to monitor the same

small section of the spectrum. Some of the auroral problems which can be tackled through such wider coverage of auroral radiation spectrum are:

- (1) The excitation mechanism of the N_2 triplet states.
- (2) The quenching rate of some of the states with relatively long radiative lifetime.
- (3) The excitation efficiency and quenching rates of



- (4) The production of NO in auroras.
- (5) The mechanism responsible for the enhancement of various N_2 emissions relative to N_2^+ emissions in relatively low altitudes (~ 90 km), red-lower border, type-B aurora.
- (6) The effect of low energy electrons and protons on the vibrational distribution of atmospheric N_2 .

ACKNOWLEDGMENTS

The author wishes to express his gratitude to NASA for providing financial assistance for this project. The success of this project can be attributed in great measure to the invaluable assistance provided by Mr. L. C. Haughney of the Airborne Science Office at NASA/Ames Research Center. Mr. Haughney arranged for the availability of both the various sets of data from different research groups which participated in NASA's 1968 and 1969 Airborne Auroral Expedition, as well as various data processing equipment.

The following scientists made their measurement available for this project and their cooperation is gratefully acknowledged:

1. Dr. S.-I. Akasofu, University of Alaska
2. Dr. K. A. Dick, Johns Hopkins University
3. Dr. R. H. Eather, Boston College
4. Professor W. G. Fastie, Johns Hopkins University
5. Dr. B. Hultqvist, Kiruna Geophysical Institute, Sweden
6. Dr. S. Mende, Lockheed Company
7. Dr. M. H. Rees, University of Colorado
8. Dr. G. J. Romick, University of Alaska

C-2

REFERENCES

- Aller, L. H. and M. L. White
1949

A. J., 54, 181.
- Banks, P. M. and T. E. Holzer
1969

J. Geophys. Res., 74, 6317.
- Banks, M. P., C. R. Chappell
and A. F. Nagy
1973

Preprint
- Banks, P. M., C. R. Chappell
and A. F. Nagy
1974

J. Geophys. Res., 79, 1459.
- Birely, J. H.
1974

Phy. Rev. A, 10, 550.
- Borst, W. L. and S. L. Chang
1972

Phys. Rev., 5, 648.
- Borst, W. L. and S. L. Chang
1973

J. Chem. Phys., 59, 5830.
- Borst, W. L. and M. Imami
1973

J. Appl. Phys., 44, 1133.
- Bowen, I. S.
1928

Ap. J., 57, 1.
- Brandt, J. C., A. L. Broadfoot
and M. B. McElroy
1965

Astrophys. J., 141, 1584.
- Broadfoot, A. L.
1967

Planet. Space Sci., 15, 1801.
- Broadfoot, A. L. and D. M. Hunten
1966

Planet. Space Sci., 14, 1303.
- Broadfoot, A. L.
1971

The Radiating Atmosphere, p. 34,
ed. M. B. McCormac, Dordrecht,
Reidel.
- Cartwright, D. C., S. Trajmar
and W. Williams
1973

J. Geophys. Res., 78, 2365.
- Chamberlain, J. W.
1961

Physics of the Aurora and Airglow
- Christensen, A. B., T.N.L. Patterson
1971

J. Geophys. Res., 76, 1764.
- Chung, S. and C. S. Lin
1972

Phys. Rev., 6, 988.
- Dalgarno, A. and M. B. McElroy
1966

Planet. Space Sci., 14, 1321.
- Deehr, C. S., A. Egeland, K. Aarsnes,
R. Amundsen, H. R. Lindalen, F.
Soraas, R. Dalziel, P. A. Smith,
G. R. Thomas, P. Staunig, H. Borg,
G. Gustafsson, L. A. Holmgren, W.
Riedler, J. Raitt, G. Skovli and
T. Weede
1973

J. Atmos. Terr. Phys., 35, 1971.
- Degen, V.
1975

Annual Report to NSF on Grant No.
9A41815X, University of Alaska.

- | | | |
|--|------|---|
| Dick, K. A., G. G. Sivjee
and H. M. Crosswhite | 1970 | <u>Planet. Space Sci.</u> , <u>18</u> , 887. |
| Dick, K. A., G. G. Sivjee,
W. G. Fastie and R. C. Schaeffer | 1971 | Technical Report No. 27, Johns
Hopkins University. |
| Eather, R. H. | 1967 | <u>Rev. Geophys.</u> , <u>5</u> , 207. |
| Eather, R. H. | 1968 | <u>J. Geophys. Res.</u> , <u>73</u> , 119. |
| Eather, R. H. and S. B. Mende | 1971 | <u>J. Geophys. Res.</u> , <u>76</u> , 1746. |
| Eather, R. H. and S. B. Mende | 1972 | <u>Advanced Study Institute on
Magnetosphere-Ionosphere
Interactions</u> , ed. Kr. Folkestad,
Univ. Press, Oslo, p. 139. |
| Elterman, L. and R. B. Toolin | 1965 | <u>Handbook of Geophysics and Space
Environments</u> , U.S. Air Force. |
| Feldman, P. D., J. P. Doering
and J. H. Moore | 1971 | <u>J. Geophys. Res.</u> , <u>76</u> , 1738. |
| Feldman, P. D. | 1973 | <u>J. Geophys. Res.</u> , <u>78</u> , 2010. |
| Feldman, P. D. and J. P. Doering | 1975 | <u>J. Geophys. Res.</u> , <u>80</u> , 2808. |
| Ferguson, E. F. | 1969 | <u>Ann. Geophys.</u> , <u>25</u> , 819. |
| Ferguson, E. E., D. K. Bohme,
F. C. Fehsenfeld and D. B.
Dunkin | 1969 | <u>J. Chem. Phys.</u> , <u>50</u> , 5039. |
| Fite, W. L. | 1969 | <u>Can. J. Chem.</u> , <u>47</u> , 1797. |
| Garstang, R. H. | 1952 | <u>Ap. J.</u> , <u>115</u> , 506. |
| Garstang, R. H. | 1956 | <u>The Airglow and the Aurora</u> , eds.
E. B. Armstrong and A. Dalgarno,
p. 324. |
| Gerard, J.-C. | 1970 | <u>Ann. Geophys.</u> , <u>26</u> , 777. |
| Gerard, J. C. | 1975 | <u>Atmospheres of Earth and Planets</u> ,
ed. B. McCormac, Reidel Pub. Co.,
p. 309. |
| Gladyshev, V. A., M. V. Jorjio,
F. K. Shuishaya, J. Crasnier
and J. A. Sauvaud | 1974 | <u>Ann. Geophys.</u> , <u>30</u> , 301. |
| Heikkila, W. J., J. D. Winningham,
R. H. Eather and S.-I. Akasofu | 1972 | <u>J. Geophys. Res.</u> , <u>77</u> , 4100. |

Henry, R. J. W., P. G. Burke and A. L. Sinfailam	1969	<u>Phys. Rev.</u> , <u>178</u> , 218.
Hultqvist, B.	1974	<u>Ann. Geophys.</u> , <u>30</u> , 223.
Jacchia, L. G.	1965	<u>Smithson. Contr. Astrophys.</u> , <u>8</u> , 215.
Keating, G. M. and E. J. Prior	1968	<u>Space Res.</u> , <u>8</u> , 982.
Keating, G. M., J. A. Mullins and E. J. Prior	1970	<u>Space Res.</u> , <u>10</u> , 439.
McConkey, J. W. and F. R. Simpson	1969	<u>J. Phys. B.</u> , <u>2</u> , 923.
McNeal, R. J. and J. H. Birely	1973	<u>Rev. Geophys. Space Phys.</u> , <u>11</u> , 633.
Mahadevan, P. and F. E. Roach	1968	<u>Nature</u> , <u>220</u> , 150.
Menzel, D. H. and L. H. Aller	1941	<u>Ap. J.</u> , <u>93</u> , 195.
Moore, J. H. and J. P. Doering	1969	<u>Phys. Rev.</u> , <u>177</u> , 218.
Nicholls, R. W.	1962	<u>J. Quant. Spectrosc. Radiat.</u> <u>Transf.</u> , <u>2</u> , 433.
Omholt, A.	1959	<u>Geophys. Publ.</u> , <u>20</u> (11).
Opal, C. B., W. K. Peterson and E. C. Beatty	1971	<u>J. Chem. Phys.</u> , <u>55</u> , 4100.
Papadopoulos, K. and T. Coffey	1974	<u>J. Geophys. Res.</u> , <u>79</u> , 674.
Peterson, R. N. and G. G. Shepherd	1974	<u>Geophys. Res. Lett.</u> , <u>1</u> , 231.
Rees, M. H.	1972	Final Report Grant NGR 06-003-110, Univ. of Colorado.
Rees, M. H. and R. A. Jones	1973	<u>Planet. Space Sci.</u> , <u>21</u> , 1213.
Rees, M. H. and D. Luckey	1974	<u>J. Geophys. Res.</u> , <u>79</u> , 5181.
Rees, M. H.	1975	<u>Atmospheres of Earth and Planets</u> , ed. B. M. McCormac, D. Reidel Pub. Co., p. 323.
Rees, M. H., G. G. Sivjee and K. A. Dick	1975	<u>J. Geophys. Res.</u> (to be published)
Riedler, W., B. Hultqvist and A. Olsen	1970	<u>Arkiv fur Geofysik</u> , <u>5</u> , 41.

Seaton, M. H.	1953	<u>Proc. R. Soc. London A.</u> , <u>218</u> , 400.
Seaton, M. H.	1955	<u>Proc. R. Soc. London A</u> , <u>321</u> , 37.
Seaton, M. H. and D. E. Osterbrock	1957	<u>Ap. J.</u> , <u>125</u> , 66.
Sharp, W. E.	1971	<u>J. Geophys. Res.</u> , <u>76</u> , 987.
Sharp, W. E. and P. B. Hays	1974	<u>J. Geophys. Res.</u> , <u>79</u> , 4319.
Shemansky, D. E.	1969	<u>J. Chem. Phys.</u> , <u>51</u> , 689.
Shemansky, D. E. and A. L. Broadfoot	1971	<u>J. Quant. Spectrosc. Radiat. Transf.</u> , <u>11</u> , 1385.
Shemansky, D. E., E. C. Zipf and T. M. Donahue	1971	<u>Planet. Space Sci.</u> , <u>19</u> , 1669.
Shemansky, D. E. and A. L. Broadfoot	1971a	<u>J. Quant. Radiat. Transf.</u> , <u>11</u> , 1385.
Shemansky, D. E. and A. L. Broadfoot	1971b	<u>J. Quant. Radiat. Transf.</u> , <u>11</u> , 1401.
Shemansky, D. E. and A. L. Broadfoot	1973	<u>J. Geophys. Res.</u> , <u>78</u> , 2357.
Sivjee, G. G.	1973	Semi Annual Report, Grant NGR 02-001-099, Univ. of Alaska.
Sivjee, G. G. and B. Hultqvist	1975	<u>Planet. Space Sci.</u> , <u>23</u> , 1597.
Sivjee, G. G. and D. J. McEwen	1976	<u>Planet. Space Sci.</u> , <u>24</u> , 131.
Smith, D. and R. A. Fouraire	1968	<u>Planet. Space Sci.</u> , <u>16</u> , 243.
Stanton, P. N. and R. M. St. John	1969	<u>J. Opt. Soc. Am.</u> , <u>59</u> , 252.
Stebbins, R. F., B. R. Turner and J. A. Rutherford	1966	<u>J. Geophys. Res.</u> , <u>71</u> , 771.
Swanson, G.	1974	Ph.D. Thesis, Univ. of Michigan at Ann Arbor.
Turner, B. R., J. A. Rutherford and D. M. J. Compton	1968	<u>J. Chem. Phys.</u> , <u>48</u> , 1602.
Vallance-Jones, A. and D. M. Hunten	1960	<u>Can. J. Phys.</u> , <u>38</u> , 458.
Vallance-Jones, A.	1971	<u>Space Sci. Rev.</u> , <u>11</u> , 776.
Vallance-Jones, A.	1974	<u>Aurora</u> , Reidel, Boston.
Vallance-Jones, A. and R. L. Gattinger	1976	<u>J. Geophys. Res.</u> , <u>81</u> , 497.

- | | | |
|---|------|---|
| Walker, J. C. G., R. S. Stolarski
and A. F. Nagy | 1969 | <u>Ann. Geophys.</u> , <u>25</u> , 831. |
| Winningham, J. R. | 1972 | <u>Earth's Magnetospheric Processes</u> ,
p. 68, ed. B. M. McCormac,
Dordrecht, Reidel. |
| Zipf, E. C. | 1969 | <u>Can. J. Chem.</u> , <u>47</u> , 1863. |